2023

Comparison of three methods of RNA extraction from human bone and RNA assessments of osteoarthritic tissue

BOSTON UNIVERSITY

ARAM V. CHOBANIAN & EDWARD AVEDISIAN SCHOOL OF MEDICINE

Thesis

COMPARISON OF THREE METHODS OF RNA EXTRACTION FROM HUMAN BONE AND RNA ASSESSMENTS OF OSTEOARTHRITIC TISSUE

by

OLIVIA HOOD

B.S., University of Minnesota, 2021

Submitted in partial fulfillment of the

requirements for the degree of

Master of Science

2023

Approved by

First Reader

Louis C. Gerstenfeld, Ph.D.
Professor of Orthopaedic Surgery

Second Reader

Beth Bragdon, Ph.D.
Assistant Professor of Orthopaedic Surgery

DEDICATION

I would like to dedicate this work to my parents Dennis and Kristie Hood who have made countless sacrifices to ensure my dreams come true.

ACKNOWLEDGMENTS

I would like to thank Dr. Gerstenfeld and Dr. Bragdon for their guidance as I completed this project. They welcomed me and mentored me as I expanded my sciences inquiry skills.

COMPARISON OF THREE METHODS OF RNA EXTRACTION FROM HUMAN BONE AND RNA ASSESSMENTS OF OSTEOARTHRITIC TISSUE

OLIVIA HOOD

ABSTRACT

The comparative analysis of gene expression in human bone can provide insight into underlying molecular mechanisms in Osteoporosis. Identifying comorbidities leading to osteoporosis and other bone metabolic diseases can lead to the discovery of therapeutic targets for human bone disease. There are significant challenges to obtaining transcriptomic data from human bone, including RNA isolation and purification from human bone. In this study, an optimized protocol for obtaining high-quality RNA from human bone samples was established, and transcriptomic data were obtained using RNA assessments to determine comorbidities of osteoporosis across different patient populations.

In this study, three methods of RNA isolation from human bone were compared. To do so, samples from 10 patients undergoing total hip arthroplasty at Boston Medical Center were collected. The three methods compared were hand-grinding human bone, using an automated tissue homogenizer to grind human bone, and 24-hour TRIzol of human bone lysates. The quality of RNA isolated using each method was determined by comparing the total yield of RNA, the purity of the RNA, the RIN value, and qPCR data assessing the average CT value for the 18s ribosomal RNA, COLA1, ALP, SOST, and DMP1 genes. Ultimately, it was found that the optimal protocol for obtaining high-quality RNA from human bone was using the automated tissue homogenizer.

The transcriptomic data in this study was generated using qPCR from high-quality RNA obtained from four patients undergoing total hip arthroplasties. The average CT and relative expression of COLA1, ALP, SOST, and DMP1 compared to 18s were used to determine comorbidities of osteoporosis. The transcriptomic data obtained revealed there are underlying mechanisms, including but not limited to age, sex, and weight for patients undergoing total hip arthroplasties. Future studies should be completed using a larger sample size to determine the underlying molecular mechanisms and comorbidities of osteoporosis.

TABLE OF CONTENTS

LIST OF TABLES

LIST OF FIGURES

LIST OF ABBREVIATIONS

ALP	Alkaline Phosphatase
BUSM	Boston University School of Medicine
BMD	Bone mineral density
BMI	Body Mass Index
cDNA	Complementary DNA
ColA1	Collagen Type I Alpha
DEXA	Dual-energy x-ray absorptiometry
DMP1	Dentin Matrix Acidic Phosphoprotein 1
GI	Gastrointestinal
MSC	Mesenchymal stem cell
PBS	Phosphate Buffered Saline
PCR	Polymerase Chain Reaction
PTH	Parathyroid Hormone
qPCR	qualitative Polymerase Chain Reaction
RANK	Receptor Activator of Nuclear Factor-κB
RIN Value	RNA Integrity Value
RT-PCR	Reverse-Transcriptase Polymerase Chain Reaction
SOST	Sclerostin
WNT	Wingless-related integration site

INTRODUCTION

Osteoporosis overview

Osteoporosis is a chronic disease caused by changes in the microstructure of bone, leading to increased porosity and low bone mineral density. This increases the risk of fracture in individuals who have osteoporosis (Yang et al., 2020). Osteoporotic fractures contribute to disability in the United States and decrease one's quality of life. As the population in the United States ages, the trajectory of osteoporotic fractures will triple in the next decade (Porter & Varacallo, 2022). Osteoporosis causes 250,000 hip fractures annually, which can be fatal (Gkastaris et al., 2020). Globally, osteoporosis is the most common bone disease. However, its cause in most individuals is idiopathic. Evidence suggests that osteoporosis has a genetic component, but these components have been complicated for scientists to identify in vivo. (Yang et al., 2020).

Bone Development

Bone is a connective tissue that is formed from the mesenchymal tissue in the developing embryo. Two processes lead to the development of bone: intramembranous ossification and endochondral ossification. Intramembranous ossification is when mesenchymal tissue directly forms bone, and endochondral ossification is when there is an intermediate of cartilage which is then replaced by bone tissue. Flat bones are formed by intramembranous ossification. These structures include the maxilla, mandible, and clavicle. Endochondral ossification forms long bones of the axial skeleton (spine) and extremities (fore and hind limbs). Bone remodeling is essential for the ossification and

growth of bone (Teti, 2011). This process involves two cellular entities: osteoblasts and osteoclasts.

Mesenchymal stem cells differentiate into osteoblasts (Figure 1). These cells form bone and secrete the extracellular matrix of bone. Once osteoblasts are surrounded by bone matrix, they are called osteocytes. These cells are only found in mature bone and facilitate communication between osteoblasts and osteoclasts to maintain bone remodeling homeostasis. Osteocytes can promote bone resorption and formation through the expression of receptor activator of nuclear factor-κB ligand (RANKL) which can activate RANK on osteoclasts to promote bone resorption (Figure 2). Or through the decreased expression of Dickkopf-related protein 1 (DKK1) and Sclerostin, that leads to bone formation by WNT-beta catenin signaling (Salhotra et al., 2020).

Hemopoietic stem cells differentiate into osteoclasts (Figure 1). Osteoclasts are multinucleated and function to resorb bone to replenish serum calcium and other mineral levels (McDonald et al., 2021). As mentioned, osteoclasts are activated by ligands binding to their receptor RANK (Figure 2). Once activated, osteoclasts bind tightly to bone, acidify the microenvironment, and release proteolytic enzymes, leading to the resorption of the mineralized matrix. This enables the release of calcium, phosphate, and collagen into the serum. Osteoprotegerin (OPG), released by osteoblasts, can act as a RANKL decoy, and bind to RANK to inhibit osteoclastogenesis (Figure 2). Ultimately, osteoblasts, osteoclasts, and osteocytes regulate each other uses paracrine mechanisms (Boyle et al., 2003).

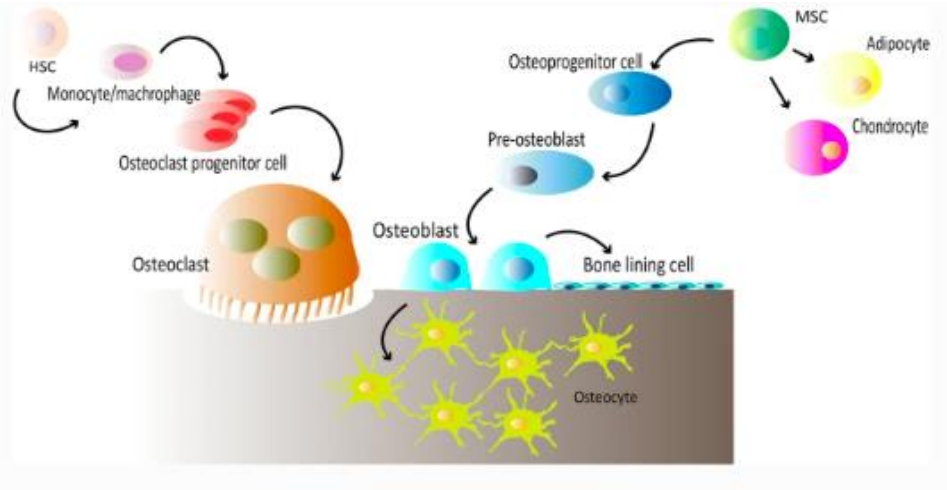

Figure 1. Development of Osteoblasts and Osteoclasts. This image obtained from Ansari et al. outlines the differentiation of osteoblasts and osteoclasts from mesenchymal stem cells and haemopoietic stem cells, respectively.

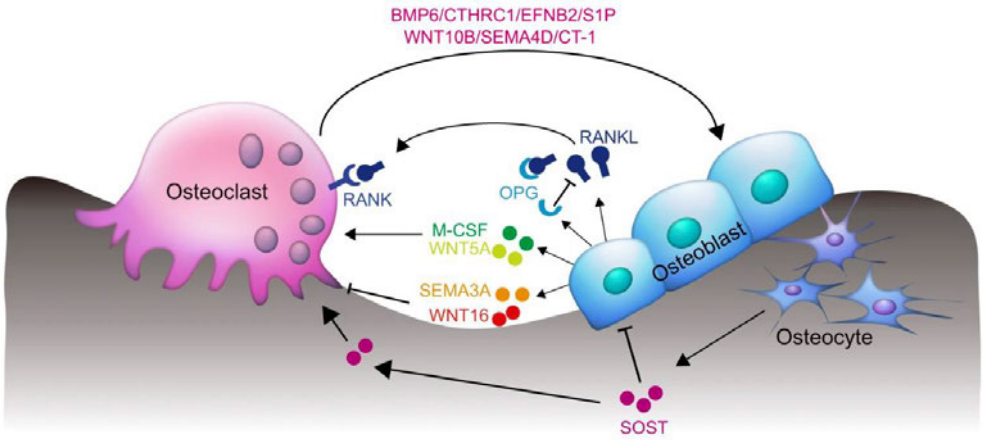

Figure 2. Paracrine Mechanisms of Osteoclasts, Osteoblasts, and Osteocytes. This figure obtained from Han et al. outlines the paracrine influence of osteoclasts, osteoblasts, and osteocytes on each other to maintain bone homeostasis.

Bone Homeostasis

Osteoclasts and osteoblasts mediate and regulate bone remodeling through the mechanism of activated osteoclasts resorbing bone and the recruited osteoblasts depositing osteoid and mineralizing the bone matrix resulting in the formation of new bone tissue (Kim et al., 2020). Bone remodeling occurs continuously throughout life to preserve the strength of bone, prevent injury, and replenish nutrient levels in the serum. Maintaining a balance between the two populations of cells is essential to maintain bone health. Disruption of the balance between osteoblasts and osteoclasts can lead to disease, including osteoporosis (Salhotra et al., 2020).

Several hormones regulate bone homeostasis, including parathyroid hormone (PTH), estrogen, and glucocorticoids. PTH is released by the parathyroid glands when serum calcium is low, in turn PTH acts on osteoclasts by upregulating RANK, leading to bone resorption. Low estrogen levels lead to a shift in bone homeostasis, where bone resorption is favored. Finally, glucocorticoids enhance osteoclast survival while decreasing osteoblasts' survival (Rowe et al., 2022). All of these factors make the bone a dynamic and sensitive connective tissue. The maintenance of bone homeostasis is essential to prevent the pathogenesis of bone.

Known causes of Osteoporosis

Several clinical factors lead to decreased bone mineral density of bone, including age, sex, and weight. While aging, the risk of developing osteoporosis increases. Bone remodeling occurs continuously as previously mentioned. As individuals age, bone absorption is favored over the formation, leading to the loss of bone. At 40 years old,

periosteal bone formation decreases, while endosteal and trabecular bone reabsorption increases. This ultimately leads to a lower overall bone mineral density in bone, decreasing its strength (See figure 3) (Demontiero, Vidal, & Duque, 2012). This demonstrates that osteoporosis is an age and sex-specific metabolic disease.

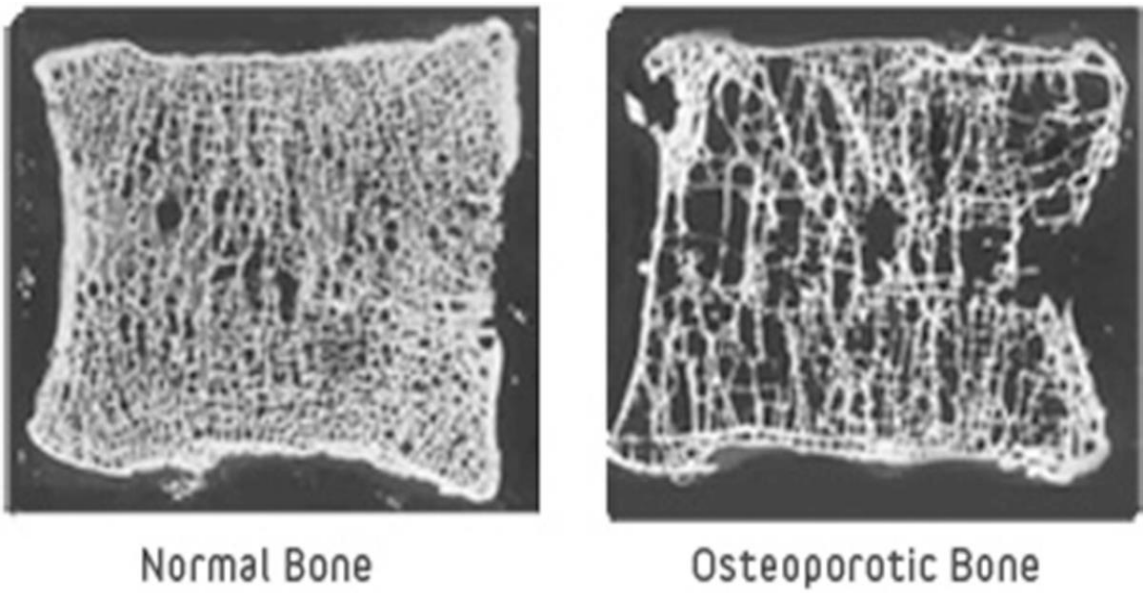

Figure 3. Histomorphometry of Normal and Osteoporotic Bone. This image was obtained from Aspray & Hill is of two slides comparing the vertebrae of a healthy 35-year-old individual (Left) and a 75-year-old with osteoporosis (Left).

As mentioned, sex predisposes individuals to osteoporosis. Decreased estrogen levels in post-menopausal women lead to increased bone remodeling, ultimately leading to bone loss (Demontiero, Vidal, & Duque, 2012). This is because estrogen decreases the bone reabsorption by altering PTH (parathyroid hormone) sensitivity to bone mass, increases calcitonin, decreases calcium excretion, and increases calcium reabsorption in the GI tract. As estrogen decreases in women, osteoclasts are more active and increase

bone absorption, and osteoblastic activity decreases, leading to less deposition of bone. At the start of menopause, trabecular bone is lost, followed by cortical bone in women (Ji & Yu, 2015). The initial loss of trabecular bone in women entering menopause causes a rapid decrease in BMD. In men, the initial loss of trabecular bone, as seen in menopausal women, does not occur. However, the gradual loss of trabecular and cortical bone does occur in men which leads to diminished BMD that is seen about a decade later than women (Ji & Yu, 2015). Therefore, the decrease in BMD in men is less significant than in women (Khosla & Riggs, 2005) (See Figure 4). Finally, oxidative stress occurs in aging, in which reactive oxygen species increase.

In a rodent model, reactive oxygen species have been found to correlate with decreased BMD. In Zhang et al., reactive oxygen species and antioxidant enzyme levels were elevated in older rats compared to younger ones. Along with increased reactive oxygen species, the BMD was significantly higher in younger rats than in older ones. Finally, they found that bone volume and trabecular thickness were elevated in older rats, and trabecular separation was significantly increased (Figure 5). Because of this, it is assumed that age-related oxidative stress correlates with age-related bone loss and osteoporosis (Zhang et al., 2011).

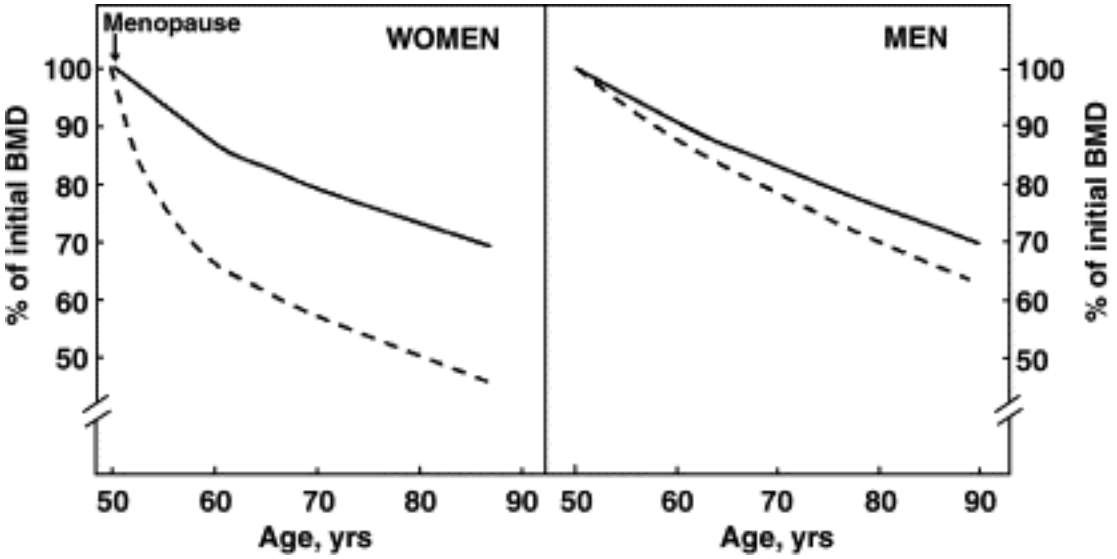

Figure 4. Age-Related Bone Loss in Women and Men. This image was obtained from Kholsa & Riggs and compares age-related bone loss in women (right) and men (left). The solid lines represent cortical bone, and the dashed lines represent trabecular bone on the graphs.

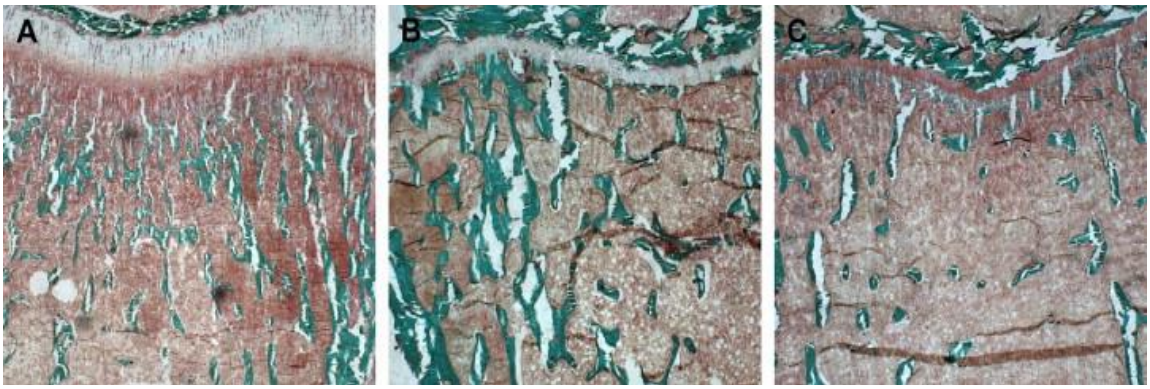

Figure 5. Tibial Histomicrographs of rats in different age groups. This image was obtained from Zhang et al. and compares the bone structures in young rats (A), Adult rats (B), and Old rats (C).

Interestingly, it has been found that weight can predispose individuals to osteoporosis. One study found that low BMI can increase the chance of osteoporosis because low BMI typically correlates with low BMD (Asomaning et al., 2006). It has been found that obesity is associated with osteoporosis. However, scientists have yet to

agree whether obesity is protective or causative of osteoporosis. Some argue that because obesity is an inflammatory disease, it may lead to the upregulation of cytokines TNF-alpha and IL-6 leading to osteoclastic activity. Also, osteoblasts and adipocytes are both derived from MSCs. Some researchers believe that with excess fat, as seen in obesity, the differentiation of MSCs into adipocytes may be favored over osteoblasts leading to decreased bone formation over time (Gkastaris, 2020).

In contrast, scientists have found that with increased body weight, BMD also increases. In a systemic review by Qiao et al., it was found that femoral neck BMD negatively correlated with osteoporosis (Qiao et al., 2020). Ultimately, scientists are still determining whether obesity correlates with osteoporosis and whether the increase in BMD in obese individuals is significant enough to offset fracture risk due to increased weight.

Secondary Osteoporosis

Secondary osteoporosis is caused by diseases or medications altering bone microstructure. Common osteoporosis-related diseases include gastrointestinal, hemochromatosis, hematological, renal, autoimmune, and endocrine disorders. Drugs such as chemotherapy agents, glucocorticoids, and immunosuppressants can also lead to osteoporosis (Mirza & Canalis, 2016). At times, secondary osteoporosis can be reversible. Patients with osteoporosis typically add more vitamin D if they are deficient. Treatment of patients with secondary osteoporosis may include lowering the dosage of medication that may be causing secondary osteoporosis. Patients should also undergo weight training exercises to facilitate bone formation. Patients may be prescribed

bisphosphonates if increased vitamin D does not improve BMD. Finally, if patients do not tolerate these forms of treatment, teriparatide may be administered via injection to combat secondary osteoporosis. This is common in patients with glucocorticoid-induced osteoporosis (Ganesan et al., 2022).

Osteoporosis and Hip Fractures

Osteoporotic hip fractures increase mortality and morbidity, making them a significant health concern. Few patients can restore full function after a hip fracture and treatment. Increased mortality and morbidity after hip fractures are associated with increased age, sex, and other health comorbidities. Therefore, it is essential to treat osteoporosis so that hip fractures can be prevented and the quality of life in elderly patients may be increased (Tai et al., 2022).

Femoral neck fractures are common hip fractures because the formal neck connects the femoral head and shaft (See figure 6). There are several types of femoral neck fractures, and each has different courses of surgical intervention (see figure 7). Very rarely do patients with a hip fracture not undergo surgical intervention. The femoral head articulates with the acetabulum, allowing for a range of motion in the hip. Displacement fractures are when the femoral head is displaced from the acetabulum. Most femoral neck fractures occur in older adults and are commonly caused by low energy falls due to low BMD or decreased mobility. The femoral artery supplies the femoral head, and these fractures can interfere with blood supply, making them dangerous. During surgical intervention, some complications may occur, including avascular necrosis.

Treatment of femoral neck fractures depends on the fracture's location and the patient's age. Young patients may undergo open-reduction internal fixation. Elderly patients will receive percutaneous cannulated screws if it is a non-displaced fracture or a total hip arthroplasty (see figure 8) or hemiarthroplasty if it is a displaced fracture (Kazley & Bachi, 2022). The optimal treatment for femoral neck fractures is still being debated due to the risks of each treatment option and the medical intervention post-surgery.

Figure 6. Pelvic Radiograph of Right hip Fracture. This is an image of a patient with a right hip fracture obtained from Kazley & Bagchi.

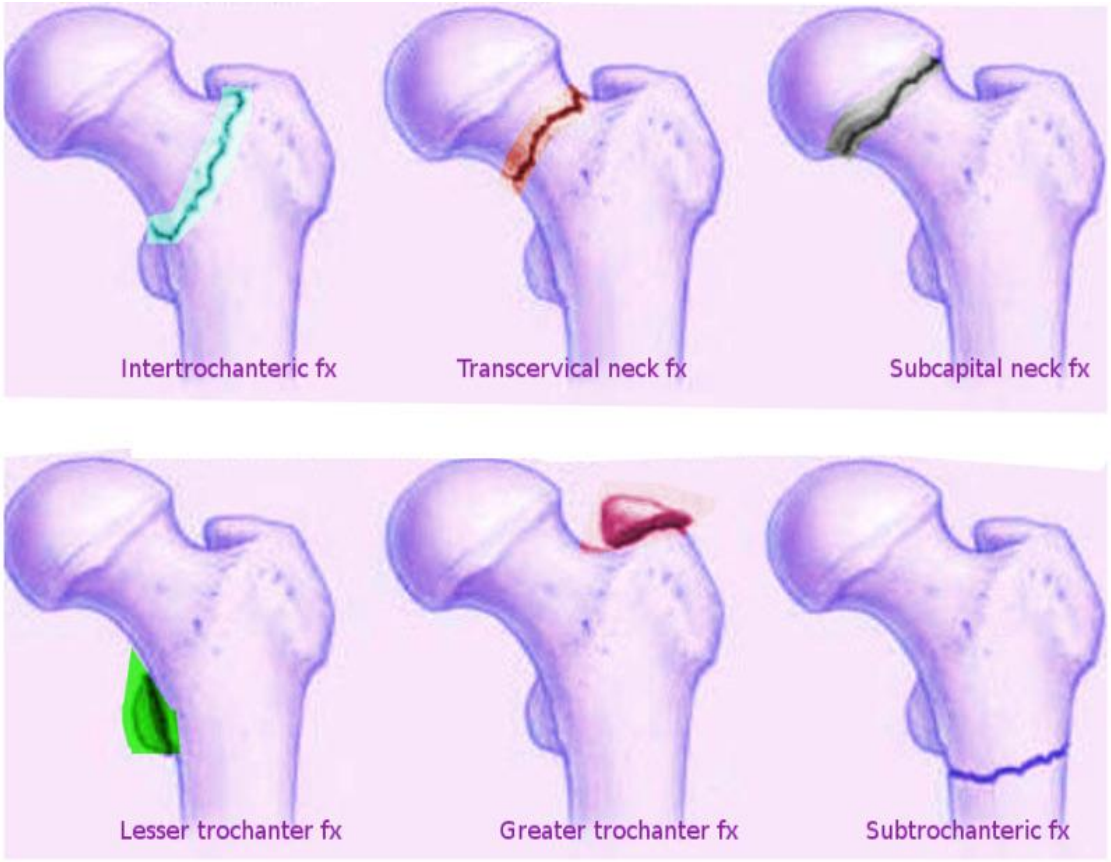

Figure 7. Different Types of Femoral Neck Fractures. This is an illustration that outlines the various types of femoral neck fractures and their locations obtained from Kazley & Bagchi.

Figure 8. Pelvic Radiograph of Right Hip Total Arthroplasty Post-Surgery. This image is of a patient's right hip after a total hip arthroplasty procedure in which the femoral head and neck were replaced and was obtained from Kazley & Bagchi.

Diagnosis and Treatment of Osteoporosis

Osteoporosis is most commonly diagnosed using radiographs or dual-energy x-ray absorptiometry (DEXA). DEXA scans to measure the BMD of the proximal femur, femoral neck, and lumbar vertebrae (Figure 9). T scores of this test compare a patient's BMD to a young adult. The Z score compares the patient's BMD to age, sex, or race. If no previous diagnosis has been made, osteoporosis may be diagnosed at the onset of a fracture. Finally, CT scans may be used to examine the cortical and trabecular bone microstructure to determine the BMD (Matzkin et al., 2019).

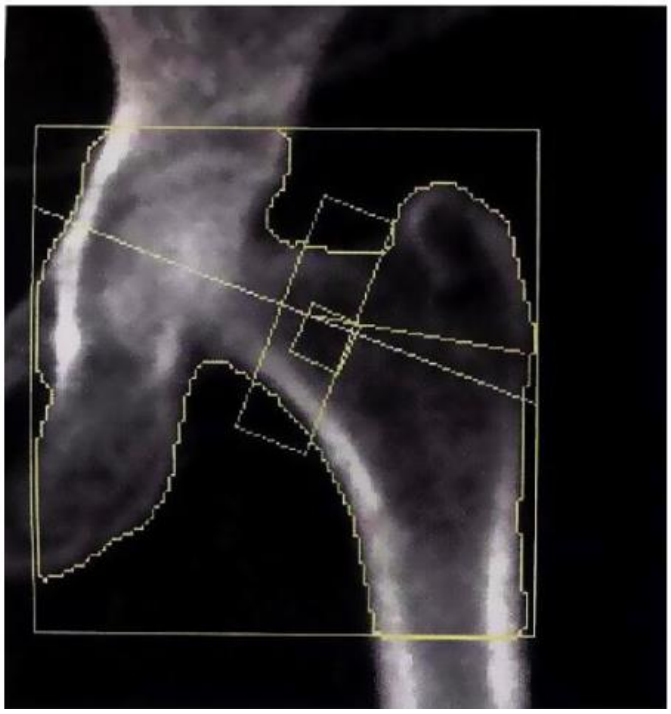

Figure 9. DEXA Scan of Osteoporotic Left Hip. This image obtained from Sowers et al. is of a DEXA scan of a hip in an osteoporotic woman. The decreased absorbance due to low BMD causes the image to be dark.

There are non-pharmaceutical and pharmaceutical interventions to treat osteoporosis. However, the non-pharmaceutical interventions encompass the prevention of the disease. This includes engaging in physical activity such as lifting weights to increase BMD. Dietary intake of healthy foods with high levels of vitamin D, calcium, and protein is also recommended. Antiosteoporosis drugs are designed to establish equilibrium between osteoblasts and osteoclasts (Zhou et al., 2020).

Pharmaceutical intervention includes calcium and vitamin D supplements, hormonal treatments, and antiresorptive therapies (Matzkin et al., 2019). As mentioned, vitamin D supplements are usually administered for secondary osteoporosis.

Antiresorptive therapy includes bisphosphonates. These drugs bind to hydroxyapatite, inhibiting osteoclastic activity, decreasing bone resorption, and increasing BMD. These drugs have decreased the risk of fractures in patients with osteoporosis. Finally, hormone treatments include estrogen receptor modulators, testosterone, and PTH. Estrogen receptor modulators prevent bone reabsorption in menopausal women. Testosterone may be administered to men if their testosterone levels are significantly low, and they may be at high risk of fracture. Finally, PTH analogs are used if patients reject the treatments listed above. PTH analogs, such as teriparatide, are administered to prevent bone reabsorption (Barnsley et al., 2021).

Efficacy and side effects of drugs

Scientists have argued that current treatments for osteoporosis lack efficacy or have significant side effects (Chen et al., 2019). Vitamin D supplements have been found to decrease the risk of hip fracture by 30% and decrease bone loss in the hip. Vitamin D is typically taken with calcium in patients with osteoporosis. However, calcium increases the risk of cardiovascular disease in excess. As mentioned, bisphosphonates are used to treat osteoporosis to manage osteoclastic activity. Bisphosphonate usage for ten years has been demonstrated to increase BMD in the femoral neck and proximal femur by 5.4% and 6.7%, respectively (Barnsley et al., 2021). However, when taken orally, these must be taken on an empty stomach, and patients must fast for an hour for them to be absorbed. It has been found that still, less than 1% of bisphosphonates taken orally are absorbed due to their short plasma half-life. These drugs may irritate the esophagus and may cause renal impairment if administered rapidly via IV (Watts & Diab, 2010). Other

adverse effects of these drugs are GI symptoms, joint pain, and atypical femoral fractures. Atypical femur fractures typically occur after five years of administration (Barnsley et al., 2021). Bisphosphonates and other anti-resorptive drugs can cause osteonecrotic jaw (Chen et al., 2019). Finally, adverse effects of hormonal treatment using selective estrogen receptor modulators, testosterone, and PTH analogs include hot flashes and cramps for estrogen, cardiovascular events for testosterone, nausea, headaches, dizziness, and pain in limbs for PTH analogs.

Osteoarthritis and Osteoporosis

Osteoarthritis is caused by the deterioration of cartilage between joints leading to pain and discomfort. While osteoporosis primarily affects the microstructure of bone, many patients clinically present with osteoarthritis and osteoporosis. In the past, it was believed that osteoarthritis and osteoporosis had an inverse relationship. However, the relationship between these degenerative diseases is unclear (Oliveira et al., 2020). In the epigenetic study of Li et al., it was found that osteoarthritis and osteoporosis have a relationship regarding gene methylation (Li et al., 2019). This indicates that a genetic component may link osteoarthritis and osteoporosis. However, underlying epigenetic or genetic causes have yet to be fully explored in patients with osteoporosis and osteoarthritis. Interestingly, patients with osteoarthritis treated with bisphosphonates, a drug used to treat osteoporosis, appeared to have less osteoarthritic pain and increased function (Xing et al., 2016). This demonstrates that the microstructure of bone may be altered in patients with osteoarthritis.

Genetics of Osteoporosis

Research has shown that osteoporotic traits are heritable, but researchers are still working to identify the individual genes responsible. There have been several genome-wide association studies of osteoporosis and single nucleotide polymorphisms. However, these studies have demonstrated that there is much more to learn about the genetics of osteoporosis (Al-Barghouthi & Farber, 2019). While there appears to be a genetic component to osteoporosis, environmental factors can also affect BMD. Genes alone, combined with environmental factors, increase the risk of fracture in osteoporosis (Trajanoska & Rivadeneira, 2019).

Osteogenesis and osteoblast differentiation is poorly understood at the molecular level. Several signaling pathways that involve osteoblastic differentiation and maturation have been identified. Many of these signaling transduction pathways have the potential to be used as diagnostic and therapeutic targets for human bone disease (Huang et al., 2007). In this study, we will be looking at the genetic expression of four genes: Collagen type 1 alpha 1 (colA1), Alkaline phosphatase (ALP), sclerostin (SOST), and Dentin Matrix protein 1 (DMP). Each of these genes have participate in the development or maturation of osteoblasts.

Genes of interest

ColA1

ColA1 has been identified as a gene that may lead to low BMD and osteoporosis (Licini et al., 2019). ColA1 codes for type I collagen, a significant component of bone. Structural abnormalities in type I collagen l, such as the formation of a homotrimer, can

lead to osteogenesis imperfecta. Typically, collagen-type I forms heterotrimers that enable bones to withstand a heavier mechanical load. Therefore, mutations in the ColA1 gene may lead to decreased BMD and increase the likelihood of developing osteoporotic tissue. (Garnero, 2015). ColA1 is highly expressed in mature osteoprogenitor cells, preosteoblasts, and fully differentiated osteoblasts. However, it is not expressed by osteocytes. Because of this, ColA1 has be identified as a marker for osteoblasts (Huang et al., 2007).

ALP

Serum ALP is a biological marker of bone formation. The ALP gene encodes for alkaline phosphatase, which is responsible for bone mineralization. (Tariq et al., 2021). Increased serum levels of ALP indicate bone remodeling and have been found to be elevated in postmenopausal female patients with osteoporosis (Tariq et al., 2019). ALP expression has also been detected in osteoblasts' differentiation (Vimalraj, 2020). Because of this, ALP is a gene of interest in this study. ALP is also highly expressed in mature osteoprogenitor cells, preosteoblasts, and fully differentiated osteoblasts. However, it is not expressed by osteocytes. Because of this, ALP has been identified as a marker for osteoblasts (Huang et al., 2007).

SOST

SOST encodes for sclerostin, a glycoprotein secreted by osteocytes, and inhibits bone formation. Interestingly, sclerostin can increase RANKL expression, which increases osteoclastic activity (Appelman-Dijkasra & Papapoulos, 2016). In one study, SOST null mice had increased BMD, formation, and strength. Interestingly, there was a

significant increase in osteoblasts but no significant change in osteoclasts. Finally, the bone formation rate of these mice was increased in the trabecular, endocortical, and periosteal bone of the femur shaft (Li et al., 2008).

DMP

It has been discovered that dentin matrix protein-1 plays a role in bone mineralization (Gluhak-Heinrich et al., 2003). Dentin matrix protein promotes normal osteocytic morphology, including maturation and attachment to lacunae (Wu et al., 2011). It has been discovered that its expression is upregulated in osteocytes when the mechanic load increases in vivo (Gluhak-Heinrich et al., 2003). In Feng et al., it was found that DMP-1 knockout mice led to poor maturation of osteocytes. The osteocytes appeared to lack dendrites which travel through canaliculi to maintain bone homeostasis. This, in turn, negatively altered the skeletal mineralization in DMP-1 knockout mice and stimulated osteomalacia (Feng et al., 2006).

Challenges of RNA assays with bone

To measure gene expression, it is essential to isolate RNA with its integrity intact. Not only is RNA relatively unstable but obtaining it from bone is complex. Researchers are still working to generate a protocol that optimizes the isolation of RNA from bone (Carter et al., 2012). When isolating RNA from bone, the bone itself must be lysed. This is because, compared to other tissues, bone has a low number of cells and is highly mineralized. Lysing the tissue enables the breakdown of mineralized tissue and cells in which RNA can be extracted. To maintain the integrity of RNA, it is essential to keep

samples on ice to avoid them thawing to room temperature as RNA degrades from room temperature (Pedersen et al., 2019).

Specific Aims

In this study, post-surgical RNA assessments will be performed of bone chips obtained from osteoarthritic femoral tissue. As mentioned, the isolation of RNA from bone has yet to be optimized, and part of this study will generate an optimal protocol to do so. Also, osteoarthritis is typically paired with osteoporosis. The underlying molecular causes of both diseases have yet to be discovered. Many times, the diagnosis of both diseases is idiopathic. The molecular understanding of these diseases will be expanded by performing RNA assessments of osteoarthritic bone.

Generation of optimized protocol

To optimize RNA extraction from bone, three extraction methods will be performed. The optimal protocol will be determined by the amount of RNA isolated, RIN values, and the quality of qPCR reactions performed using the five genes previously discussed.

RNA assessment of osteoarthritic tissues

The second aim of this study is to expand the molecular understanding of osteoporosis by looking for possible comorbidities. To do so, bone chips from acetabular reamings were obtained from several patients undergoing total hip arthroplasty. For each patient, qPCR was done to determine the expression of COLA1A, ALP, DMP-1, and SOST. The demographics of these patients were recorded to determine if there is a possible correlation between sex, age, BMI, or smoking history and osteoporosis. Patients

with secondary osteoporosis due to systemic glucocorticoid usage, chemotherapy, sickle cell disease, rheumatoid arthritis, and bone metabolic drugs were excluded from this study to increase the reliability and validity of the results.

METHODS

Informed consent and Tissue Collection

All research was carried out under an Institutional Research Board approved protocol. All HIPAA guidelines were adhered to by the research team involved in the study. One week before surgery ten patients undergoing total hip arthroplasty which met the study inclusion/exclusion criteria were contacted by phone. The goals of the study and uses of surgical discard tissues that were collected for this study were reviewed with each patient. If the patient agreed to participate, formal consent was obtained from patients two hours before the surgery, again reviewing and answering any additional questions the patient might have. At this time the patient's signature was obtained on the consent form.

The femoral neck and head were removed during the surgery, and acetabular reamings were obtained by the orthopedic surgeons. The tissues were placed in a sterile disposable specimen cup and placed in a cooler containing ice. The tissues were transported back to the lab within 15 minutes after being removed from the patient.

Patient Demographics

The comorbidities that exist for six of the ten patients used in this study were collected from the chart review at the time of phone consent to complete the comorbidities portion of this study. The limited set of patient demographics used in this study are listed in Table 1.

Table 1. Patient Demographics for 6 Samples

Sample ID	Age	Sex	Race	BMI	Smokes (Yes/No)	A1C Range
287	76	Male	White	34.3	Former	5.4
294	41	Female	Hispanic	24.1	No	4.7
297	56	Male	White	28.4	No	5.1
299	63	Female	White	26.9	Former	5.1
300	65	Female	White	20.3	No	5.3
305	50	Female	NA	26.9	No	5.5

Note. Samples were obtained from 6 patients undergoing total hip arthroplasty surgery. The demographics of these patients were considered along with RNA assays to determine comorbidities that exist for osteoporosis and other bone metabolic disease.

Tissue Preparation

Once brought to the laboratory, the acetabular reamings were placed into a sterile 500 mL pyrex jar (1397-500) and washed with a solution containing 10 mL of 100x Antibiotic-Antimycotic solution (Gibco 15240062) and 100mL of Dulbecco's phosphate buffered saline (D-PBS). The jar was vigorously shaken to rinse the reamings and was filtered using a sterile stainless steel cell dissociation sieve (Sigma-Aldrich CD1-1KT). The reamings were squeezed using a sterile stainless-steel spatula (Sigma S3897-1EA) to force any blood cell elements through the sieve. The reamings were then transferred into a second sterile 500 mL pyrex jar to avoid loss of reamings. The reamings were rewashed with the solution containing 10 mLs of antibiotic-antimycotic solution and 100 mL of DPBS.

Bone Chip Preparation and Collection

The 500 mL pyrex jar containing the reamings was placed on ice, and the reamings were transferred to a disposable culture dish (Falcon 353025) and placed on ice. A sterile forceps was used to obtain 100 mg of bone chips. Each bone chip obtained was placed into liquid nitrogen. Once the desired amount of bone chips were obtained, extra bone chips and reamings were flash-frozen in liquid nitrogen and kept in the freezer at -80 ° C.

Hand Grinding Bone Protocol

The 100 mg of bone placed in liquid nitrogen was immediately ground into a powder-like substance using an autoclaved pestle and mortar. Liquid nitrogen was added as needed to avoid sublimation from the mortar. The ground bone and liquid nitrogen were kept in a slurry. Once the bone was ground entirely, it was transferred evenly to three 2 mL Eppendorf tubes, and 750 µL of TRIzol Reagent (Fischer 15596026) was added to the three tubes. The tubes were mixed by flicking the tube and then submerged in liquid nitrogen for 5-10 seconds. A 5 mm stainless-steel bead (Qiagen 69997) was ejected into each tube. The tubes were placed in a pre-cooled tissue sample holder kept at -20° C overnight before the experiment to ensure the samples were kept at a slurry-like consistency. The tissue sample holder was then clamped into a Qiagen Tissue Lyser II machine, and the tissue was lysed at 30 Hz for 2 minutes, or until the samples were adequately lysed.

Once removed from the tissue lyser, the microcentrifuge tubes were transferred to ice, and each tube and its contents were transferred to two new sterile 2 mL microcentrifuge tubes containing 0.5 mL of TRIzol. The solution was left on ice for 2 minutes, and then 200 µL of 1- Bromo-3-chloropropane (Sigma MKCH2273) was added to each tube. The tubes were vortex and transferred on ice to be centrifuged for 15 minutes at 14000 rpm at 4° C.

After being centrifuged, the microcentrifuge tubes were removed from the centrifuge and placed on ice. Two layers formed in the tube, and the aqueous phase (top, transparent layer) was pipetted into a new, sterile 1.5 mL microcentrifuge tube. The volume was typically 500 µL, and an equal volume of chilled isopropanol was added to the microcentrifuge tube. The tubes were inverted to mix the aqueous phase and isopropanol. The tubes were then centrifuged for 30 minutes at 14000 rpm at 4° C.

After being centrifuged, the liquid (roughly 1 mL) was removed from each microcentrifuge tube using a micropipette. 500 µL of chilled ethanol was aliquoted into each of the microcentrifuge tubes. The tubes were centrifuged for 5 minutes at 14000 rpm at 4° C. The 500 µL of ethanol was removed using a micropipette. If a pellet was visible, caution was taken so it would not be disturbed. After removing the ethanol, 500 µL of chilled ethanol was added to the tube and was centrifuged for 5 minutes at 14000 rpm at 4° C. After this, a pellet was visible at the bottom of the tube, and the liquid was removed from the tube without disturbing it. The tubes were left on ice for two minutes to allow excess ethanol to evaporate, but caution was taken to avoid over-drying the pellet. The

pellets were resuspended in UltraPure DNase/RNase-Free Distilled Water (Thermo Fisher 10977023) and combined into one 1.5 mL microcentrifuge. The final volume of the tube was 60 μL. The extracted RNA was flash-frozen in liquid nitrogen by submerging the tube in liquid nitrogen using forceps. The RNA was then stored in the freezer at -80° C.

Homogenizer protocol

200 mg of bone chips were obtained from acetabular reamings washed with Antibiotic-Antimycotic and DPBS, as previously described. The bone chips were placed in liquid nitrogen and then transferred to a 50 mL conical (Corning 352070) containing 5 mL of TRIzol (Fischer 15596026). The conical containing the sample in TRIzol was left on ice for 2 minutes. The conical was then submerged in liquid nitrogen for 10 seconds so that the solution would have a slurry-like consistency. Using a ring stand and clamps, the Powergen 700 Homogenizer (Fisher Scientific 006060714) was plugged and held in place. The 150 and 850 Hand Held Homogenizer Accessory Stainless-Steel Probe (Fischer 15340173) was attached to the homogenizer to grind the bone. The 50 mL conical tube was kept on ice, and the homogenizer was lowered until it was submerged in the TRIzol-bone solution. The machine was turned on, and the tissue was homogenized until the bone chips had been ground into a powder-like solution, and the solution became opaque. The solution was kept in a slurry-like consistency the entire time.

The homogenized bone chips were then transferred to size 2 mL sterile microcentrifuge tubes. 750 µL of TRIzol (Fischer 15596026) was added to each tube. The tubes were flicked to mix the solution and then submerged in liquid nitrogen to be kept at a slurry consistency. A 5 mm stainless-steel bead (Qiagen 69997) was ejected into each tube. The samples were then placed in a pre-chilled tissue sample holder that had been stored at 20 ° C overnight. The steps following this are the same as in the hand-ground bone method previously described.

24 Hour TRIzol Storage

200 mg of bone chips were obtained from acetabular reamings washed with Antibiotic-Antimycotic and DPBS, as previously described. The bone chips were placed in liquid nitrogen and then transferred to a 50 mL conical (Corning 352070) containing 3 mL of TRIzol (Fischer 15596026). The conical containing the sample in TRIzol was left on ice to allow the bone chips to thaw. The bone chips were then homogenized on ice using the Powergen 700 Homogenizer (Fisher Scientific 006060714) as previously described for two minutes. The conical containing the TRIzol/Lysate mixture was left on ice for 3-4 minutes to allow a sludge-like material to settle at the bottom of the conical. 1 mL of the TRIZol/lysate mixture was transferred into sterile 1.5 mL microcentrifuge tubes, and the sludge was avoided. The tubes were spun down at 4° C, 1200 g for 10 minutes. The lysates were transferred to new 1.5 mL microcentrifuge tubes, and the sludge at the bottom was avoided. The microcentrifuge tubes were stored at -80° C for 24 hours.

After 24 hours, the lysate samples were thawed on ice. For every 1 mL of TRIzol/lysate, 0.2 mL chloroform (ThermoFischer, J67241-AP) was added. The microcentrifuge tubes were shaken to mix the chloroform/TRIzol lysate solution. The microcentrifuge tubes sat at room temperature for 3 minutes, and then spun down at 4° C, 12000 g for 15 minutes. The aqueous layer was removed from the microcentrifuge tube and transferred to a new one. Equal volume of ethanol was added. The samples were then loaded onto the Qiagen RNeasy Mini Kit (cat #74104) column starting at step #3.

RNA Purification

After initial extraction RNA stored at -80° C was thawed on ice. The RNA sample was purified using the Qiagen RNeasy Mini Kit (Qiagen 74104). This was done to remove DNA and other contaminants. The reagents used in this protocol were kept on ice, as was the sample, to prevent RNA degradation. The protocol provided in the RNeasy Mini kit handbook was used to purify the sample. Once the RNA samples were purified, the sample was stored in the freezer at -80 ° C.

Spectrophotometry

The concentration of RNA was obtained using the NanoDrop 2000c Spectrophotometer (Thermo Scientific ND-2000). The software was installed on the computer, and the "nucleic acid test" was selected as "RNA." To blank the machine, 1 µL of UltraPure DNase/RNase-Free Distilled Water (Thermo Fisher 10977023) was pipetted on the machine. The "measure" button was pressed, and the spectrophotometer measured the concentration of the sample. The water concentration was always close to 0, ensuring

the accuracy of the machine. Once the machine was blank, 1 μL of the RNA sample was loaded onto the machine, and its concentration, 260/280, wavelength, and absorbance were obtained. The data was transported to Microsoft Excel.

RNA Integrity Number Determination

The RIN value of each sample was obtained by sending 2 μL of purified RNA from each sample to BUSM's Microarray & Sequencing Resource Core Facility for RNA Bioanalyzer analysis. QC and RIN values were collected.

RT-PCR

Reverse transcriptase polymerase chain reaction (RT-PCR) was completed to generate cDNA (complementary DNA). 0.2-2 μg of RNA was removed from the sample tubes stored at -80° C and pipetted into a 0.6 mL microcentrifuge tube. Additional DEPC treated water was added to the RNA to have a final volume of 10.4 μL. The reagents $MgCl_2$ (Applied Biosystems 1719713), dNTP Mix (Applied Biosystems 1847937), 10X RT Buffer (Applied Biosystems 1687775), and Random Hexamers (Invitrogen 2132105) were thawed on ice, combined in a 1.5 mL microcentrifuge tube, and vortexed with the ratios listed below (Table 2).

Table 2. Reagents and their Desired Ratios to Make cDNA from RNA extracted from Human Bone.

Reagent	Sample Volume (µL)
$MgCl_2$	6.61
dNTP	6.0
10X RT Buffer	3.0
Random Hexamers	1.5

Note. The reagents listed in this table were combined in an microcentrifuge tube to make cDNA from RNA extracted from human bone in this experiment.

RNase inhibitor (Applied Biosystems 566719) and TaqMan Reverse Transcriptase (Applied Biosystems 00844083) were thawed on ice and mixed by flicking the tube. The enzymes were spun down and mixed into the 1.5 mL microcentrifuge tube containing the reagents listed previously with the ratios listed below (Table 3).

Table 3. Enzymes and their Desired Ratios Used to Make cDNA from RNA Extracted from Human Bone.

Enzyme	Sample volume (µL)
RNase Inhibitor	0.6
TaqMan Reverse Transcriptase	1.89

Note. The enzymes in this table were used to produce cDNA from RNA extracted from human bone in this experiment in the amount specified.

The final volume of RT-PCR reagents was 19.6 µL, and it was added to the 0.6 mL microcentrifuge tube containing 10.4 µL of RNA to yield a final volume of 30 µL. The tube was inverted and flicked to mix the solution. The tubes were transferred to a GeneAmp PCR System 9700 Thermal Cycler (Applied Biosystems). The cycle setting on the machine was as followed: 25° C for 10 minutes, 37° C for 60 minutes, 95° C for 5 minutes, and 4° C on HOLD indefinitely. Once the cycle was completed, the cDNA was diluted 1:50 and stored at -20° C until used.

Preparation of Samples for qPCR

To perform quantitative polymerase chain reaction (qPCR), only TaqMan reagents were used. For each sample of RNA, the five primers listed below were thawed on ice and flicked to mix (Table 4). A primer mix containing Universal Master Mix and the desired primer was made in a separate 1.5 mL microcentrifuge tube. In a separate 1.5 mL microcentrifuge tube, cDNA diluted with in UltraPure DNase/RNase-Free Distilled Water (Thermo Fisher 10977023) for a final concentration of 1:10 was added. The primer/Master Mix solution had a final volume of 11 µL per well in the 96-well plate, and the diluted cDNA sample had a final volume of 9 µL per well. The specific reagents used and their desired amounts are listed below (Table 5). The solutions in both microcentrifuge tubes were pipetted up and down to mix before being added to a 96-well PCR plate (Thermofisher Scientific 00472427). While loading the samples into each well the reagents were kept on ice, and the pipette tip was switched for each primer and each sample. Real-time PCR compatible MicroAmp Optical Adhesive Film (Applied

Biosystems 335NAC) was added to the 96-well plate, and it was centrifuged for 2 minutes at 1500 rpm. The plate was then placed in the Applied Biosystems StepOnePlus Real-Time PCR machine (4376600). The qPCR cycle was as follows: 50° C for 2 minutes, 95° C for 10 minutes, 95 ° C for 15 seconds (repeat 40 times), 60° C for 1 minute.

Table 4. RNA Assay Primers.

Primer	Assay ID	Catalog Number	Distributor
RNA18 S	Hs05282140_g1	4351372	ThermoFisher Scientific
COL1A1	Hs00164004_m1	4331182	ThermoFisher Scientific
ALPL	Hs01029144_m1	4331182	ThermoFisher Scientific
SOST	Hs00228830_m1	4331182	ThermoFisher Scientific
DMP1	Hs01009391_g1	4331182	ThermoFisher Scientific

Note. The primers listed were used for qPCR. The 45s primer was used a house keeping gene, while the additional four primers were for genes of interest.

Table 5. Desired Amount of each Reagent per well for qPCR.

Reagent	Volume/ Well(µL)
Diluted cDNA	9
Master Mix	10
Desired Primer	1

Note. The reagents and their desired amount are listed below. Each well of the 96-well plate had the same amount of cDNA, Master Mix, Primer, and Water.

qPCR Computer Set up and Results Collection

The StepOne v2.3 software was used to perform RT qPCR on the genes of interest. One the software, the instrument selected was the "StepOnePlus instrument (96 wells". The type of experiment selected was "Quantitation- Comparative CT". The reagents selected was "TaqMan Reagents". Finally, the speed selected was "Standard ~2 hours". Once the wells of the 96-well plate were labeled on the software with the specific sample ID and primer used, the "Start Run" button was pressed. After the run, using Microsoft Excel, the average CT value for each gene was recorded. The $2^{-\Delta C_T}$ value was calculated to determine the relative expression of each gene compared to the 18s gene.

RESULTS

RNA Quantity of the 3 Conditions

To determine the best method for isolating RNA from human bone, the total yield of RNA extracted from each patient was calculated by multiplying the concentration of purified RNA determined by spectroscopy by the total volume. The Total yield of RNA was determined from the following extraction methods: hand grinding the bone, using the homogenizer, or storing the homogenized bone in TRIzol and purifying the RNA one day later. The total RNA yield results are recorded in Figure 10.

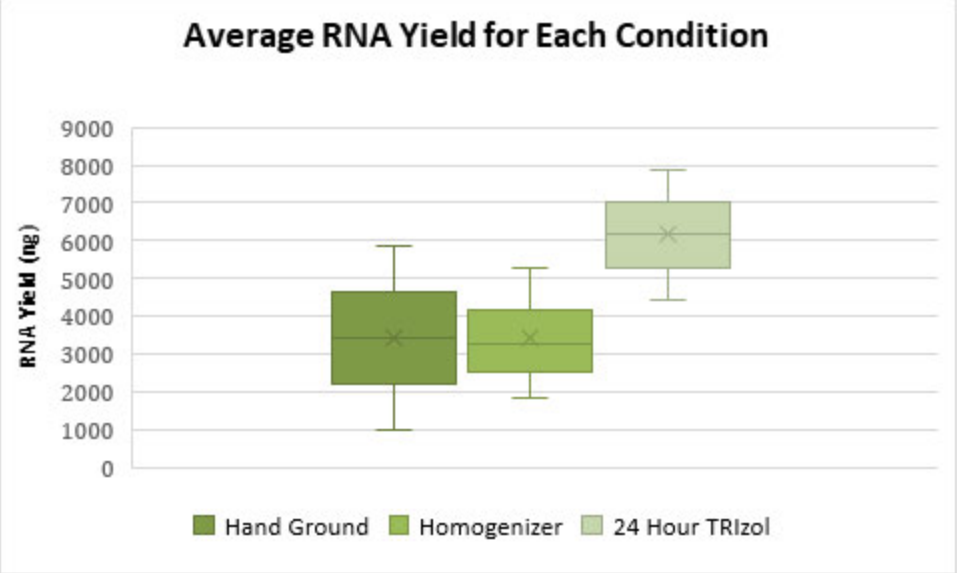

Figure 10. **Average RNA Yield for Each Extraction Method.** The yield of RNA extracted from each sample of human bone that was hand ground, homogenized, or stored in TRIzol overnight and purified the next day was obtained. The average was then calculated for each of the conditions.

RNA Purity of the 3 Conditions

UV spectroscopy measured each RNA sample's purity at 230, 260, and 280 nm by the BU Microarray and Core Facilities. The average absorbance for each extraction method is listed in Table 6.

Table 6. Average Absorbance Ratio for Each Method of RNA Extraction from Human Bone.

Method of Extraction	260/280 Average Absorbance	260/230 Average Absorbance
Hand Ground	**2.01**	**1.02**
Homogenizer	**1.96**	**1.60**
24 Hour TRIzol Storage	**1.80**	**1.00**

Note. The absorbance ratio of each sample was determined for each method of extraction and averaged to determine which method yielded the purest RNA.

RIN Values of Each Sample

The BU Microarray and Core Facilities determined the RIN value of each patient sample. RIN values range between 1-10, where 10 is the highest quality. High-quality RNA has a RIN of ~8.0. The RIN values for each sample were used to determine the best method of RNA isolation from human bone.

The RIN value for each patient for hand-ground bone is listed in Table 7. The RIN value for each patient in a side-by-side comparative experiment of hand grinding bone and using the homogenizer is listed in Table 8. Finally, the RIN value for each patient in a side-

by-side comparative experiment of using the homogenizer and storing ground bone in TRIzol is listed in Table 9.

Table 7. Hand Ground Bone RIN Values.

Sample ID	RIN
287	5
294	4.6
297	2.4
299	7
300	8.2
305	6

Note. The RIN value of each sample hand-ground was obtained to determine the best method of RNA extraction from human bone and to determine what samples could be used for RNA assays in this experiment.

Table 8. Side by Side Comparison of the RIN for Hand Grinding and Homogenizer Methods.

Sample ID	RIN	Method of Extraction
307	5.6	Hand Ground
307	5.5	Homogenizer
308	5.2	Hand Ground
308	4.1	Homogenizer

Note. The RIN values of two samples were obtained to compare the hand-grinding method to the homogenizer method. This was done to determine the best method of RNA extraction from human bone and to determine what samples could be used for RNA assays in this experiment.

Table 9. Side by Side Comparison of the RIN for Homogenizer Methods and TRIzol Storage.

Sample ID	RIN	Method of Extraction
306	3.3	Homogenizer
306	Undetermined	TRIzol Storage
309	Undetermined	Homogenizer
309	Undetermined	TRIzol Storage

Note. The RIN values of two samples were obtained to compare the hand-grinding method to the homogenizer method. This was done to determine the best method of RNA extraction from human bone and to determine what samples could be used for RNA assays in this experiment.

qPCR data of 5 Genes for a Comparative Analysis of RNA Extraction Methods

Average CT Values of 5 genes for Each Sample Hand Ground or Homogenized

To determine the relative quality of the RNAs from human bone, qPCR was conducted to perform a side-by-side comparative analysis. qPCR was conducted to assess the expression of 5 genes: 18s, COLA1, ALP, SOST, and DMP1. The three methods tested were hand-grinding the bone, using the homogenizer, and storing the ground bone remains for 24 hours in TRIzol. The average CT value of each gene to compare hand grinding to the homogenizer can be found in Table 10.

Table 10. Side by Side Comparison of the Average CT Value of 18s, COLA1, ALP, SOST, and DMP for Hand Grinding and Homogenizer Methods.

Sample ID	18s	COLA1	ALP	SOST	DMP1	Extraction method
307	12.54	23.73	28.02	35.06	31.81	Hand Ground
307	12.21	22.83	27.78	33.88	31.54	Homogenizer
308	13.74	24.92	28.13	33.74	31.72	Hand Ground
308	12.82	23.22	26.97	32.38	30.66	Homogenizer

Note. The average 18s gene CT value of each sample that RNA was extracted by hand grinding and by homogenizing the bone is listed in this table. The 18s CT values were then used as a reference to determine the relative expression of four other genes, and to determine the best method of RNA extraction.

Relative Expression of Genes for Samples Hand Ground or Homogenized

In conjunction with the average CT value and RIN of each sample, the relative expression of each gene compared to 18s for samples hand-ground and homogenized. In this experiment, qPCR of the four genes enables the analysis of the integrity of the mRNA to ultimately determine the best method of RNA extraction from human bone. The relative expression of ALP, COLA1, DMP, and SOST compared to 18s for patient 307 can be seen in figures 11, 12, 13, and 14, respectively. The relative expression for these genes for patient 308 can be seen in figures 15, 16, 17, and 18, respectively. Both samples that had been processed using the homogenizer had higher gene expression than the hand-ground samples.

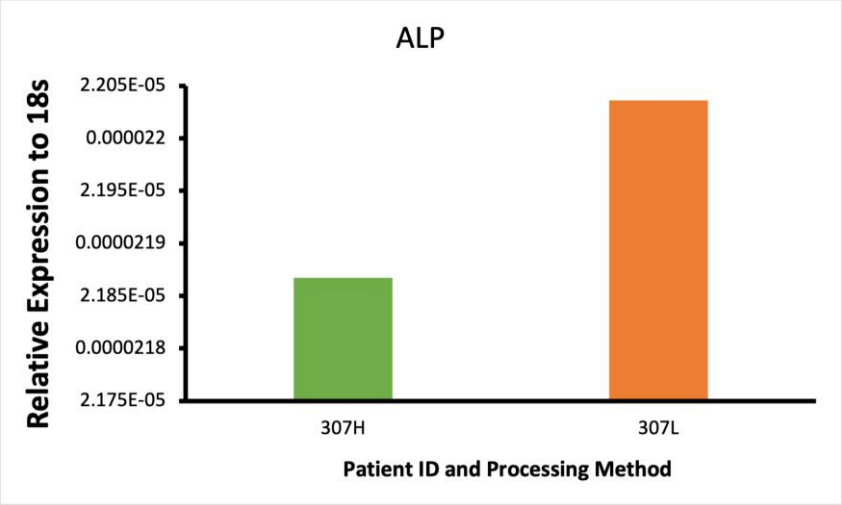

Figure 11. Comparison of ALP Relative Expression to 18s Expression for Hand ground and Homogenized Bone from Patient 307. The 18s gene was used as a housekeeping gene during qPCR. The 2^-ΔCT value for the patient (y-axis) is shown in this graph. The hand ground sample is green and labeled with the sample ID number and "H". The homogenized sample is orange and is labeled with the sample ID number and "L".

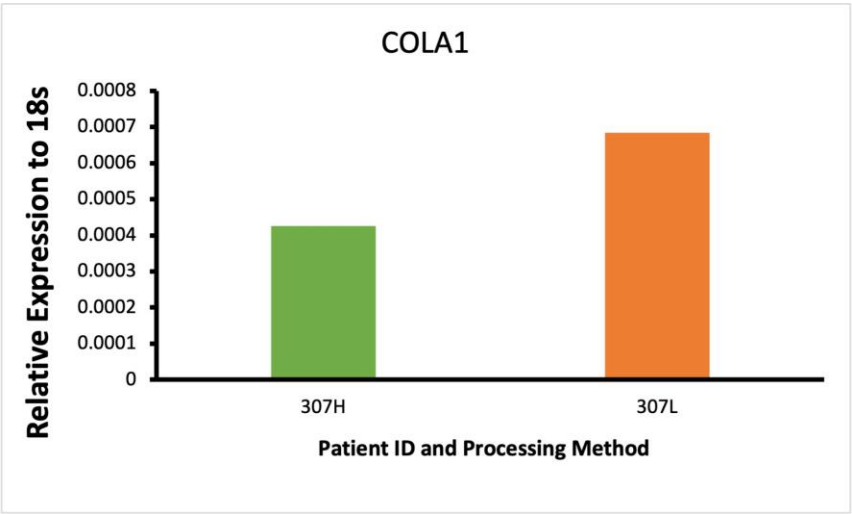

Figure 12. Comparison of COLA1 Relative Expression to 18s Expression for Hand ground and Homogenized Bone from Patient 307. The 18s gene was used as a housekeeping gene during qPCR. The 2^-ΔCT value (y-axis) is shown in this graph. The hand ground sample is green and labeled with the sample ID number and "H". The homogenized sample is orange and is labeled with the sample ID number and "L".

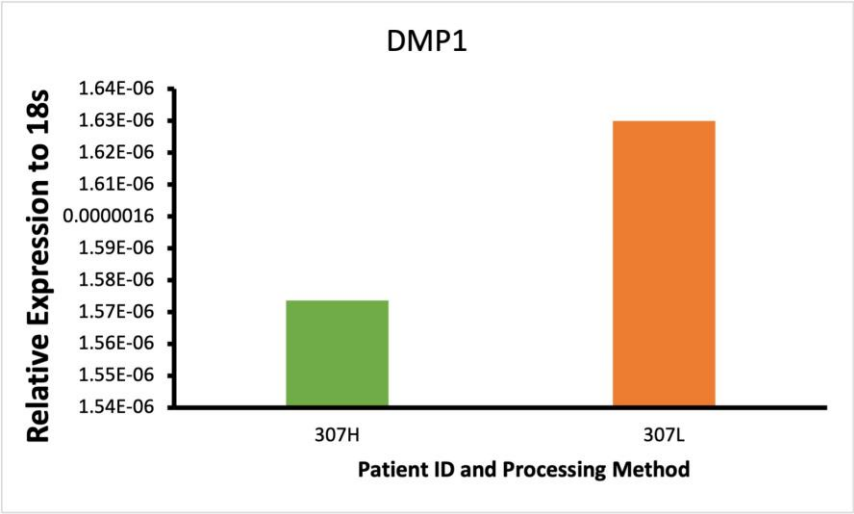

Figure 13. Comparison of DMP1 Relative Expression to 18s Expression for Hand ground and Homogenized Bone from Patient 307. The 18s gene was used as a housekeeping gene during qPCR. The 2^-ΔCT value (y-axis) is shown in this graph. The hand ground sample is green and labeled with the sample ID number and "H". The homogenized sample is orange and is labeled with the sample ID number and "L".

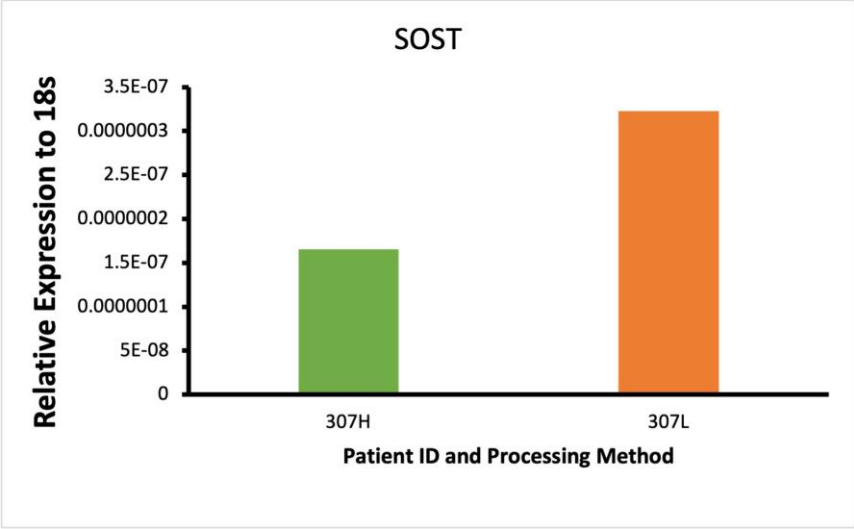

Figure 14. Comparison of SOST Relative Expression to 18s Expression for Hand ground and Homogenized Bone from Patient 307. The 18s gene was used as a housekeeping gene during qPCR. The 2^-ΔCT value (y-axis) is shown in this graph. The hand ground sample is green and labeled with the sample ID number and "H". The homogenized sample is orange and is labeled with the sample ID number and "L".

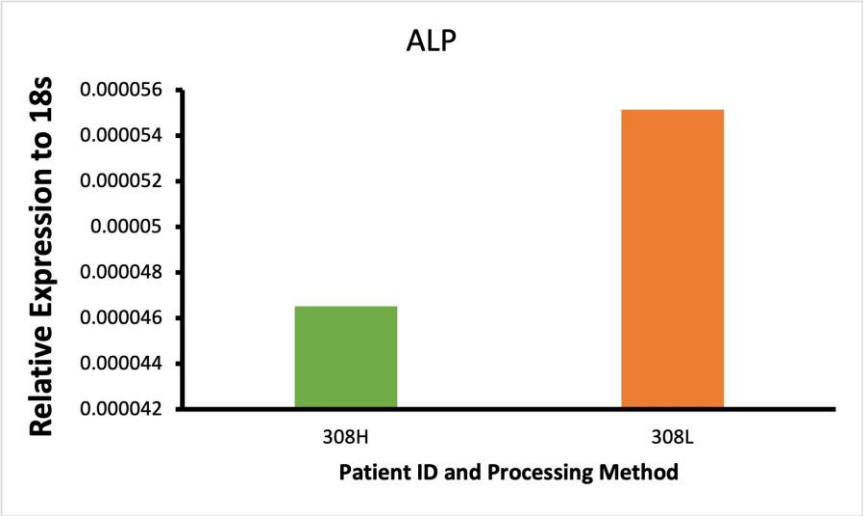

Figure 15. Comparison of ALP Relative Expression to 18s Expression for Hand ground and Homogenized Bone from Patient 308. The 18s gene was used as a housekeeping gene during qPCR, and the 2^-ΔCT value for each patient is on the y-axis of this graph. The hand ground sample is green and labeled with the sample ID number and "H". The homogenized sample is orange and is labeled with the sample ID number and "L".

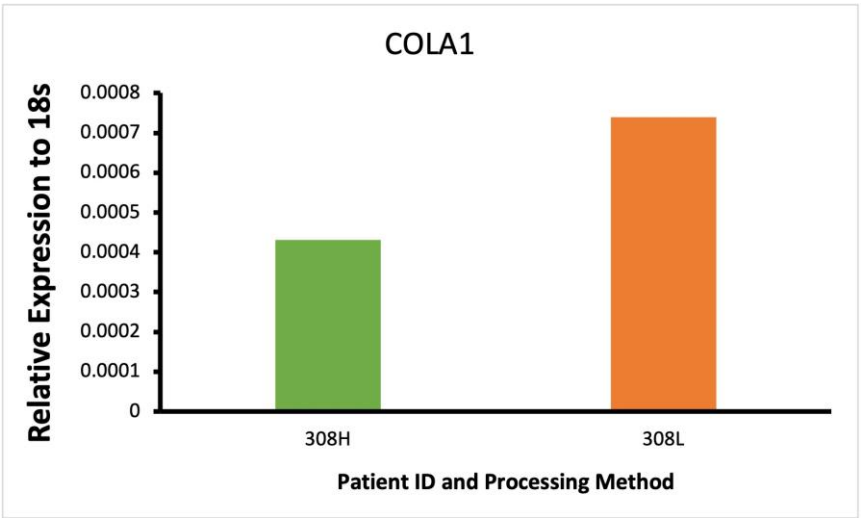

Figure 16. Comparison of COLA1 Relative Expression to 18s Expression for Hand ground and Homogenized Bone from Patient 308. The 18s gene was used as a housekeeping gene during qPCR. The 2^-ΔCT value for each patient (y-axis) is shown in this graph. The hand ground sample is green and labeled with the sample ID number and "H". The homogenized sample is orange and is labeled with the sample ID number and "L".

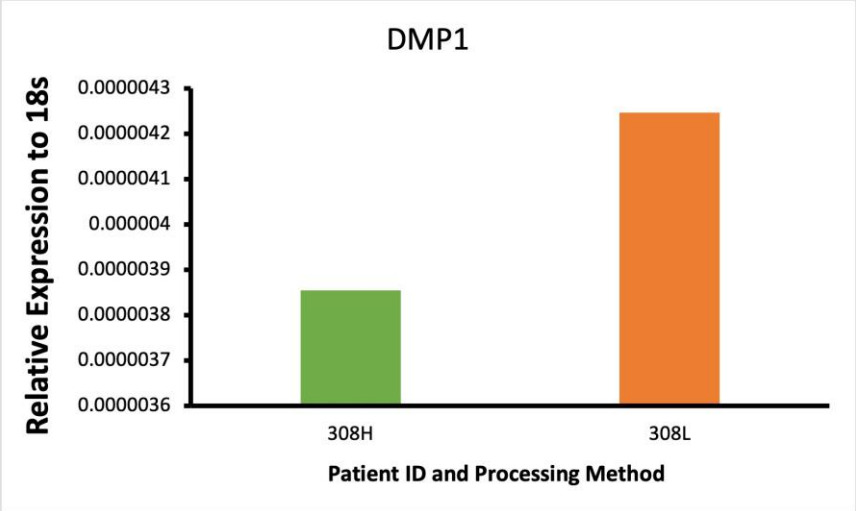

Figure 17. Comparison of DMP1 Relative Expression to 18s Expression for Hand ground and Homogenized Bone from Patient 308. The 18s gene was used as a housekeeping gene during qPCR. The 2^-ΔCT value for each patient is shown in this graph. The hand ground sample is green and labeled with the sample ID number and "H". The homogenized sample is orange and labeled with the sample ID number and "L".

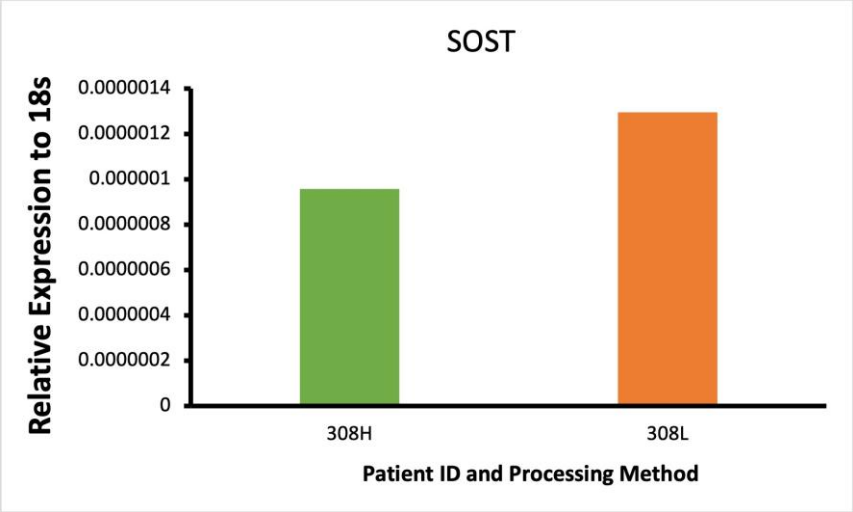

Figure 18. Comparison of SOST Relative Expression to 18s Expression for Hand ground and Homogenized Bone from Patient 308. The 18s gene was used as a housekeeping gene during qPCR. The 2^-ΔCT value for each patient (y-axis) is shown in this graph. The hand ground sample is green and labeled with the sample ID number and "H". The homogenized sample is orange and is labeled with the sample ID number and "L".

Average CT Values for 5 genes of Each Sample Homogenized or Stored in TRIzol

To determine the best method of RNA extraction from human bone, the average CT values for the 18s, COLA1, ALP, SOST, and DMP1 genes were determined for samples 306 and 309. A side-by-side comparison was made to determine if using the homogenizer or storing it in TRIzol for 24 hours was more efficient. The average CT value for each gene and the extraction method are listed in Table 11.

Table 11. Side by Side Comparison of the Average CT Value of 18s, COLA1, ALP, SOST, and DMP for Homogenizer Methods and TRIzol Storage.

Sample ID	18s	COLA1	ALP	SOST	DMP1	Extraction method
306	13.72	23.29	27.77	34.52	31.31	Homogenizer
306	23.88	35.47	35.66	Undetermined	37.16	TRIzol Storage
309	12.76	24.38	28.68	32.46	31.51	Homogenizer
309	13.83	24.86	29.33	33.45	31.72	TRIzol Storage

Note. The average 18s gene CT value of each sample that RNA was extracted by homogenizing and by storing the ground reamings in TRIzol is listed in this table. The 18s CT values were then used as a reference to determine the relative expression of four other genes, and to determine the best method of RNA extraction.

Relative Gene Expression of 4 Genes Compared to 18s

A comparative analysis of the mRNA extracted using the homogenizer or 24-hour TRIzol storage was conducted using qPCR and determining the $2^{-\Delta C_T}$ value for each patient. To further analyze the quality of the RNA extracted from human bone, the relative expression of each gene compared to 18s was determined using qPCR. The

relative expression of ALP, COLA1, DMP1, and SOST for patient 306 can be seen in Figures 19, 20, 21, and 22, respectively. The relative expression of ALP, COLA1, DMP1, and SOST for patient 309 can be seen in Figures 23, 24, 25, and 26, respectively.

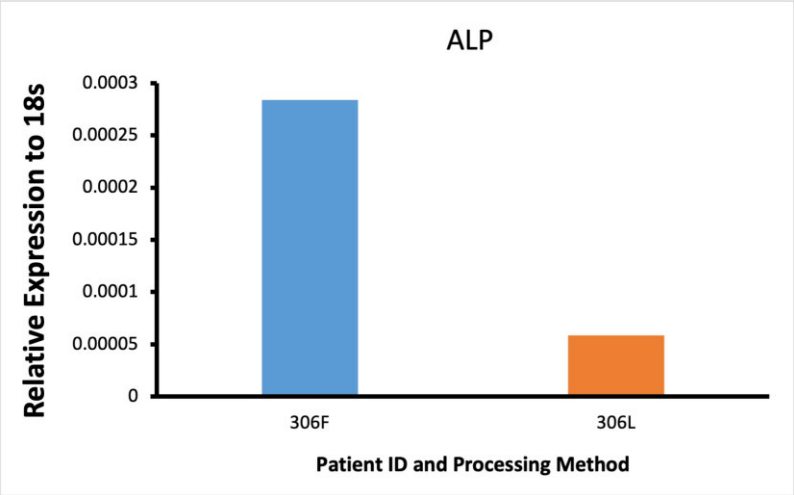

Figure 19. Comparison of ALP Relative Expression to 18s Expression for TRIzol Stored and Homogenized Bone from Patient 306. The 18s gene was used as a housekeeping gene during qPCR. The 2^-ΔCT value for each patient (y-axis) is shown in this graph. The sample stored in TRIzol for 24 hours is blue and labeled with the sample ID number and "F". The homogenized sample is orange and labeled with the sample ID number and "L".

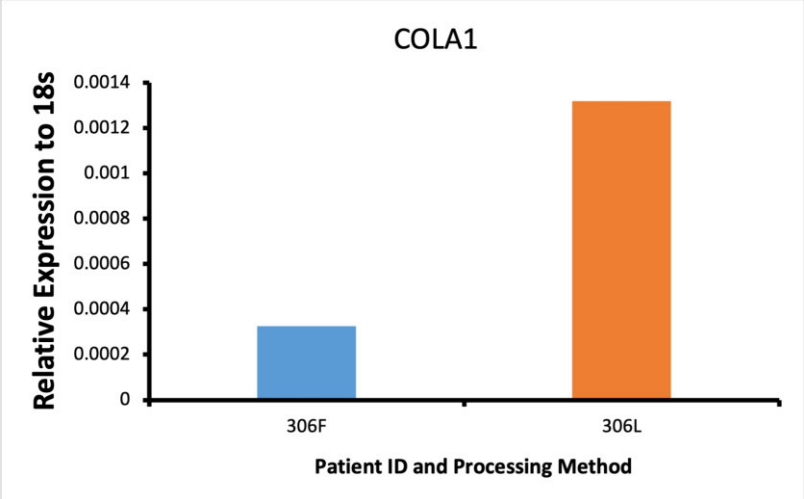

Figure 20. Comparison of COLA1 Relative Expression to 18s Expression for TRIzol Stored and Homogenized Bone from Patient 306. The 18s gene was used as a housekeeping gene during qPCR. The 2^-ΔCT value for each patient (y-axis) is shown in this graph. The sample stored in TRIzol for 24 hours is blue and labeled with the sample ID number and "F". The homogenized sample is orange and labeled with the sample ID number and "L".

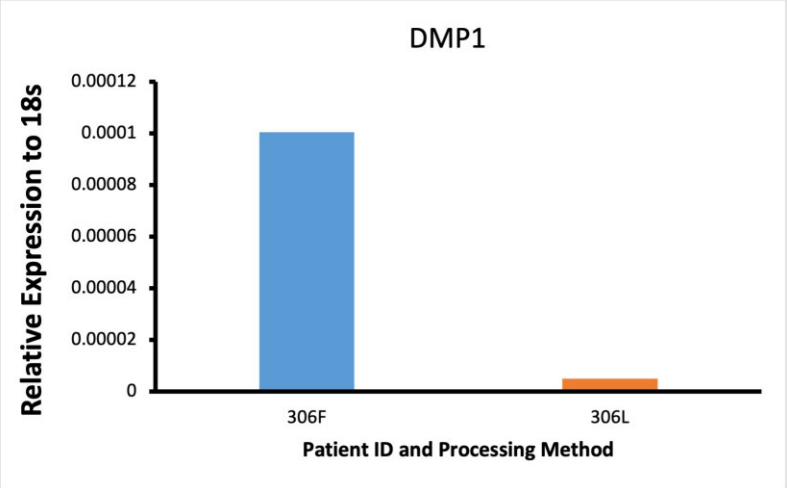

Figure 21. Comparison of DMP1 Relative Expression to 18s Expression for TRIzol Stored and Homogenized Bone from Patient 306. The 18s gene was used as a housekeeping gene during qPCR. The 2^-ΔCT value for each patient (y-axis) is shown in this graph. The sample stored in TRIzol for 24 hours is blue and labeled with the sample ID number and "F". The homogenized sample is orange and labeled with the sample ID number and "L".

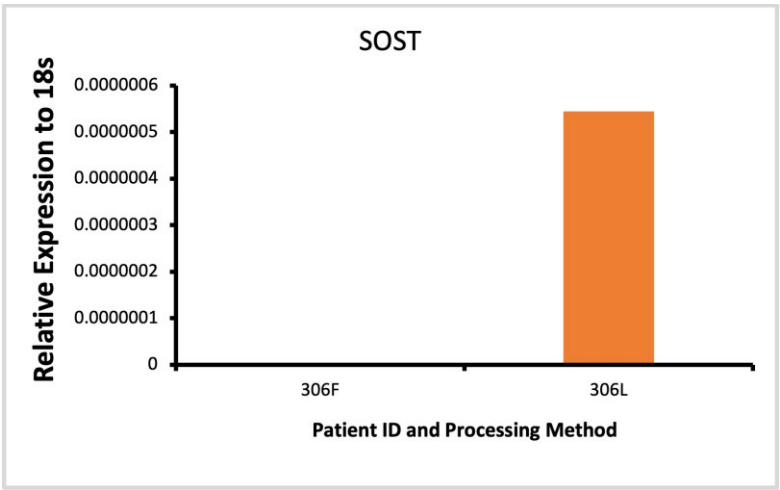

Figure 22. Comparison of SOST Relative Expression to 18s Expression for TRIzol Stored and Homogenized Bone from Patient 306. The 18s gene was used as a housekeeping gene during qPCR, and the 2^-ΔCT value (y-axis) is shown in this graph. The sample stored in TRIzol for 24 hours is blue and labeled with the sample ID number and "F". The homogenized sample is orange and labeled with the sample ID number and "L". SOST expression was undetermined for 306F.

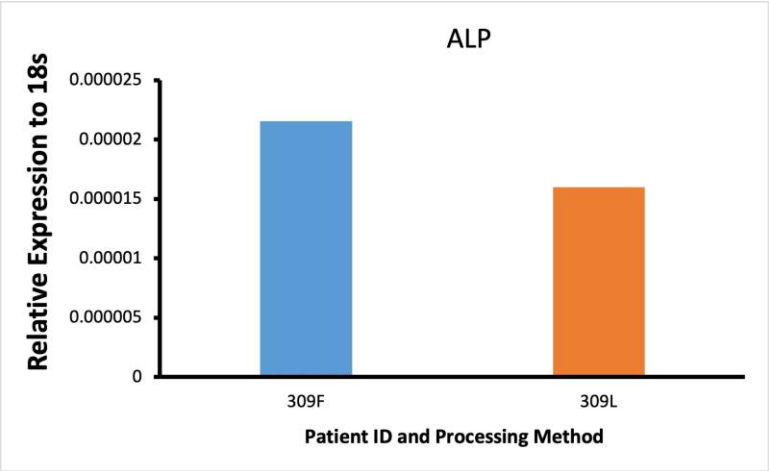

Figure 23. Comparison of ALP Relative Expression to 18s Expression for TRIzol Stored and Homogenized Bone from Patient 309. The 18s gene was used as a housekeeping gene during qPCR. The 2^-ΔCT value for each patient (y-axis) is shown in this graph. The sample stored in TRIzol for 24 hours is blue and labeled with the sample ID number and "F". The homogenized sample is orange and labeled with the sample ID number and "L".

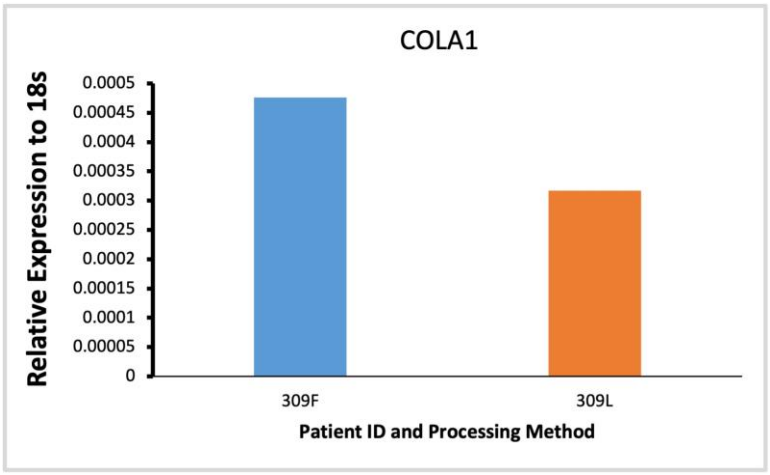

Figure 24. Comparison of COLA1 Relative Expression to 18s Expression for TRIzol Stored and Homogenized Bone from Patient 309. The 18s gene was used as a housekeeping gene during qPCR, and the 2^-ΔCT value for each patient (y-axis) is shown in this graph. The sample stored in TRIzol for 24 hours is blue and labeled with the sample ID number and "F". The homogenized sample is orange and labeled with the sample ID number and "L".

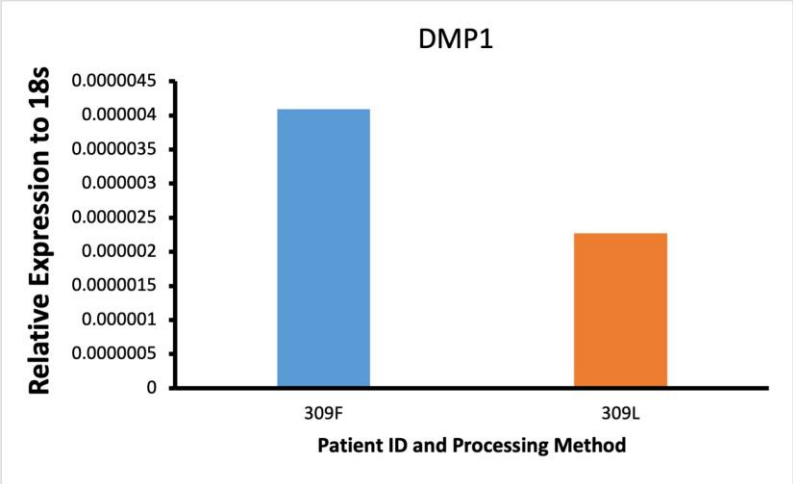

Figure 25. Comparison of DMP1 Relative Expression to 18s Expression for TRIzol Stored and Homogenized Bone from Patient 309. The 18s gene was used as a housekeeping gene during qPCR. The 2^-ΔCT value for each patient (y-axis) is shown in this graph. The sample stored in TRIzol for 24 hours is blue and labeled with the sample ID number and "F". The homogenized sample is orange and labeled with the sample ID number and "L".

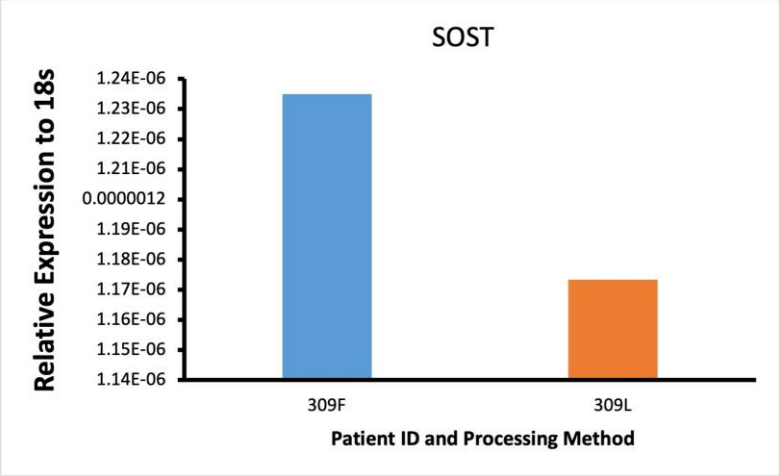

Figure 26. Comparison of SOST Relative Expression to 18s Expression for TRIzol Stored and Homogenized Bone from Patient 309. The 18s gene was used as a housekeeping gene during qPCR. The 2^-ΔCT value for each patient (y-axis) is shown in this graph. The sample stored in TRIzol for 24 hours is blue and labeled with the sample ID number and "F". The homogenized sample is orange and labeled with the sample ID number and "L".

qPCR Data For 6 Hand Ground Samples to Determine Comorbidities of Osteoporosis

Average CT Values of 5 genes for Each Sample Hand Ground

To identify comorbidities of osteoporosis, the average CT values for the 18s, COLA1, ALP, SOST, and DMP1 genes were determined for 6 samples. The average 18s CT value for patient 299 was high, indicating RNA degradation, and the qPCR machine could not identify the CT values for this sample. One of the 18s CT values for patient 305 was high and may have caused the data to be skewed. Because of this, patient 299 was omitted from this part of the study. The average CT value for each gene and the sample ID are listed in Table 12. Each patient's demographics can be found in Table 1 of the methods section.

Table 12. Average CT Value of 18s, COLA1, ALP, SOST, and DMP for 6 Samples.

Sample ID	18s	COLA1	ALP	SOST	DMP1
287	12.76	24.73	28.13	33.49	34.10
294	11.71	25.40	28.88	35.30	35.79
297	13.48	25.98	30.82	33.75	36.61
299	32.08	Undetermined	Undetermined	Undetermined	Undetermined
300	12.13	26.93	30.43	34.34	36.20
305	14.42	24.63	30.16	33.67	31.76

Note. The average 18s gene CT value of each sample was obtained from 6 patient RNA samples that were extracted by hand grinding human bone. The average18s CT value was used as a reference gene to determine the relatively expression of each gene to identify comorbidities of osteoporosis

Relative Gene Expression of 4 Genes Compared to 18s for 6 Samples

To identify comorbidities of osteoporosis, RNA assays were performed to identify osteoporosis comorbidities to determine the relative expression of ALP, COLA1, DMP1, and SOST compared to the 18s gene. The CT value of each sample was obtained using qPCR, and the $2^{-\Delta C_T}$ value was calculated. The ideal range for the 18s rRNA CT value was predetermined to be between 10 and 15. Any sample with an 18s CT value outside this range was excluded from this study portion. As mentioned, patient 305 had an outlying 18s CT value, which was excluded from this portion of the study. The relative expression of the 4 genes compared to 18s for each sample can be seen below in Figure 27.

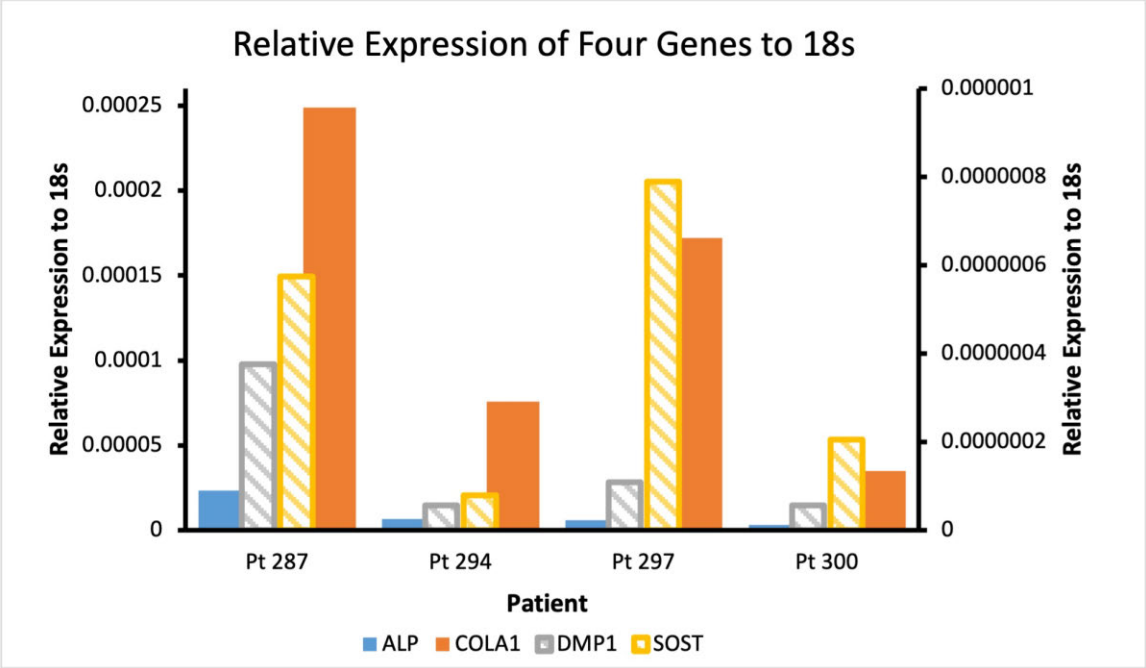

Figure 27. Relative Expression of ALP, COLA1, DMP1, and SOST Compared to 18s. The 18s gene was used as a housekeeping gene during qPCR. The 2^-ΔCT value for each patient is shown in this graph on the y-axis. The left-hand scale measures the 2^-ΔCT value for ColA1 and ALP. The right-hand scale measures the 2^-ΔCT value for DMP1 and SOST. Patients 299 and 305 were excluded from this graph.

DISCUSSION

RNA Yield from Each Condition

According to Figure 10, the samples stored in TRIzol for 24 hours had the highest RNA yield. This method also slightly varied the amount of RNA obtained from each sample. The hand-ground bone samples had a higher average RNA yield compared to using the homogenizer. However, the hand-ground samples' RNA yield varied compared to the homogenizer.

The variation in the amount of RNA obtained by hand grinding the bone could be due to several factors. First, hand grinding the bone depends on the technique. Different individuals processed the human bone samples. Some used sheer force by pressing and rotating the pestle to grind the bone, while others used compressive force by forcefully moving the pestle upwards and downwards to grind the bone. Second, the processing time for hand grinding the bone varied significantly. Some samples were ground rapidly and efficiently, while others took longer. Finally, while hand grinding the bone, bone loss occurs due to splashing while using the pestle and mortar. At times, the force of the pestle caused some powdered bone to splash out of the mortar and could not be reobtained due to the risk of contamination.

It must be noted that using the homogenizer had a similar but lower median value for the amount of RNA obtained compared to hand-grinding the sample. The smaller range of variation may be because the homogenizer ground each sample with the same force, leading to less user error and deviation in the results. Because of this, using the homogenizer is likely more reliable than hand grinding.

RNA Purity

The absorbance level was used to determine if protein, phenols, and other contaminants were contaminated in the purified RNA. The 260/280 ratio was used as a primary indicator of purity to determine if there was a presence of proteins or other contaminants that absorb near 280 nm. The 260/230 was used as an indicator to decide if carbohydrates or phenols were in the sample, causing an absorbance around 230 nm. The desired value for the 260/280 and 260/230 ratio is ~2.0 to be determined as "pure" RNA. Chemical compounds like TRIzol in this experiment may contaminate RNA and alter the 260/280 and 260/230 ratios (Krebs et al., 2009).

The hand-ground samples had the purest RNA according to the 260/280 average absorbance. However, the Homogenizer had the purest RNA 260/230 average absorbance (Table 6). The 260/280 absorbance was 1.96 for the homogenizer. Because its 260/230 ratio was much higher than the hand-ground sample, 1.60 compared to 1.02, the homogenizer was determined to be the best method to obtain pure RNA.

The hand-ground samples likely had a low 260/230 absorbance due to leftover TRIzol, ethanol, or isopropanol. To avoid this in the future, the pellet of RNA should be dried for a more extended time before resuspending it in water.

The 24-hour TRIzol storage had low 260/280 and 260/230 average absorbance compared to the other methods. It is possible that because the sample was stored in TRIzol, more carried over to the column when purifying the RNA. To avoid this in the future, the RNA samples may need to be washed and resuspended in water several times

after being purified. Though this method had the highest yield of RNA, the lack of purity makes this method less reliable than hand-grinding the bone and using the homogenizer.

RIN Values

Overall, the hand-ground samples had the highest RINs compared to the homogenizer (Table 8). When looking at the RIN values of the homogenizer compared to the 24-hour TRIzol storage, the RIN could not be obtained for the 24-hour storage and one sample for the homogenizer (Table 9). Because of this, it is difficult to determine the best RNA extraction method among the three methods.

Samples obtained from patient 307 had very similar RINs. The hand-ground sample had a RIN of 5.6, and the homogenizer sample had a RIN of 5.5. However, the samples obtained from patient 308 had RINs of 5.2 and 4.1 for the hand-ground and homogenized samples, respectively (Table 8). More samples should be obtained and compared to determine the best method to obtain high-integrity RNA.

It must be noted that there may have been personal errors when obtaining the RIN for each sample. Given that samples 306F, 309F, and 309H were all sent to the core together and all had inconclusive results, it is possible the RNA was degraded due to improper storage of the samples. This is likely because the samples were obtained from different patients at different times and were processed using different methods.

According to BUSM's Microarray & Sequencing Resource Core Facility for RNA Bioanalyzer, the 24-hour TRIzol storage samples 306F, 309F, and 309H showed an abnormally high smear in the 5s region, leading to abnormal results on the bioanalyzer. It is assumed that there was either a high amount of small RNA or degradation of rRNA.

Thus, interfering with the RIN number. These samples may be used for RNA-seq to determine gene expression.

RIN Values and qPCR CT Values

As mentioned, to determine the best method of RNA extraction from human bone, RNA assays were performed, and the CT value of the 18s, ALP, COLA1, DMP1, and SOST genes were determined (Table 10). This was done in addition to obtaining the RIN for each sample because the RIN is measured by estimating RNA integrity using gel electrophoresis, and the 28s and 18s ribosomes are examined to determine a ratio (Puchta et al. 2020). However, the RIN does not directly measure to mRNA integrity of the sample.

Interestingly, the samples hand-ground and homogenized had similar 18s CT values. The bone homogenized from patients 307 and 308 had a lower 18s CT value than the hand-ground sample and the expression of COLA1, ALP. SOST, and DMP1 (Table 10). Though the RINs for the side-by-side experiment comparing the homogenizer to TRIzol storage could not be obtained, the qPCR data revealed CT values for the 18s gene and COLA1, ALP, SOST, and DMP1. The homogenized samples had lower 18s CT values than the TRIzol storage samples (Table 11). Patient 306 had a high 18s CT value of 23.88, and it was determined that the sample was degraded. However, the patient sample 309, which was homogenized as well as stored in TRIzol, had an 18s CT value of 12.76 and 13.83, respectively.

Patients with low RINs obtained in this study did not always have high average 18s CT values. This is demonstrated by patient 308 and 306 homogenized samples.

However, as seen in the demographics portion of this study for patient 299, a high RIN did not always generate a low average 18s CT value.

Best Processing Method Conclusion

Using the amount of RNA obtained, purity of the RNA, the RIN value, and average CT values obtained in this study, it was determined that the best method to process human bone is using the homogenizer. This method yielded less RNA, but its purity was the highest compared to the others. The RIN values and qPCR data were suitable for future demographic studies. This method also yields less variation in the results, making it the most reliable method.

Comorbidity Analysis

As mentioned, patients 299 and 305 were excluded from the demographic comorbidities portion of this study due to the 18s CT values. Because the samples had high RIN values, it is assumed that they had either degraded when making cDNA or had an error with the reagents.

Overall, each patient had high COLA1 expression compared to all other genes. ALP expression was lower than COLA1 but higher than DMP1 and SOST expression. SOST appeared to have higher expression compared to DMP1. Interestingly, all patient samples followed this trend when analyzing the qPCR data (Figure 27). Because of this, it was concluded that all patient samples had a more osteoblastic phenotype than osteocytic (Huang, 2007).

Patient 287 had the highest expression of COLA1, ALP, and DMP1 compared to all other samples (Figure 27). According to Table 1, this patient had a BMI of 34.3 and is

considered to be obese. Interestingly, these results are consistent with other research findings. In patients suffering from obesity, the cytokines leptin and adiponectin are released in excess. Previous studies have demonstrated that leptin and adiponectin directly influence osteoblasts and osteoclasts. Additionally, increased leptin leads to increased mRNA expression and protein levels of COLA1 and ALP (Hou et al., 2020). Therefore, this patient's excess fat may promote the release of excess leptin, leading to a more osteoblastic cellular profile.

Another possible explanation for this patient's increased expression of COLA1, ALP, and DMP1 is that the increased mechanical load on this patient's joints may facilitate bone formation so the skeleton can withstand the body weight. These two explanations can be explored further using a larger group of patients.

In contrast, patient 300 had the lowest expression of ALP and COLA1 compared to the other patients (Figure 27). According to Table 1, this patient had a BMI of 20.3 and considered to be underweight. Body weight and BMD are positively correlated, indicating that this patient likely has low BMD and a higher fracture risk. This is because bone mass is lost with a low mechanical load on the patient's skeleton (Hou et al., 2020).

Additionally, given that this patient is a post-menopausal woman, she likely has low estrogen levels, which leads to bone resorption due to the alteration of PTH and increased activity of osteoclasts. Because of this, trabecular bone is lost, followed by the loss of cortical bone, which may have led to low expression of ALP and COLA1 compared to other patients (Ji & Yu, 2015). To determine if this patient has low BMD, a DEXA scan of the hip can be used to measure this patient's BMD compared to a patient

with normal BMD. Furthermore, other patients' BMD can be measured using a DEXA scan to the effects of age, sex, and BMI on BMD. Finally, more patients should be used in this study and compared to validate the findings in this study.

Patient 297 had the highest expression of SOST compared to the other patients and a high expression of COLA1 (Figure 27). As mentioned, SOST is mainly secreted by osteocytes and is a marker for this cell population. SOST expression is elevated by glucose. However, this patient had an A1C value of 5.1 (Table 1). Other factors that upregulate SOST expression include age, Vitamin D, glucocorticoids, and Runx2 (Vasiliadis, 2022).

From the demographics obtained in Table 1, it is difficult to deduce why SOST may be elevated. However, studies have shown that increased sclerostin leads to hip joint deterioration (Azzam et al., 2019). Looking at Figure 27, patient 297 has a very high expression of SOST compared to patients 287 and 300, who had higher SOST expression than the other patients. Interestingly, the average age for patients undergoing a hip total arthroplasty procedure is 67. Patient 297 is only 56 years old. Patients 287 and 300, who had elevated SOST, but not nearly as high of expression as patients 297, were ages 76 and 65, respectively.

Therefore, the elevated SOST expression in this patient may have led to the deterioration of the hip joint, resulting in the need for premature total hip arthroplasty. Finally, according to Table 1, this patient had a BMI of 28.4, and is considered to be overweight. As previously discussed, this may explain the increased expression of

COLA1. More patients should be used in this study to support the findings from this patient's results, and more patient history should be obtained.

Patient 294 had the lowest expression of SOST and DMP1 compared to the other patients, indicating that this patient had little osteocytic expression (Figure 27). When looking at Table 1, this patient had an A1C value of 4.7, which was lower than any other patient. The A1C value corresponds with the glucose level in the body and indicates this patient has a lower average glucose level than the other patients in this study. As previously mentioned, SOST expression positively correlates with glucose levels. Therefore, it is likely that this patient had the lowest level of SOST expression compared to the other patients in this study because of her low A1C value.

DMP1 facilitates the mineralization of bone. Patients with low DMP1 expression or mutations in this gene can develop brittle bones, osteomalacia, or hypophosphatemic rickets (Feng et al., 2006). When looking at Table 1, the patient is significantly younger than all other patients in this study. As mentioned, the average age of patients undergoing a total hip arthroplasty surgery is 67. However, this patient is 41 years old. Therefore, it is possible that the low expression of DMP1 caused poor bone formation and mineralization, resulting in the need for premature total hip arthroplasty. To corroborate these findings, more patients should be examined.

To conclude, in Figure 27, the expression of COLA1 is higher in men than in women. Additionally, the expression of COLA1 positively correlates with BMI. Therefore, it is evident that bone metabolic diseases are sex, age, and weight dependent.

In the future, a more extensive correlational study involving patients undergoing total hip arthroplasty would be useful in identifying comorbidities of bone metabolic disease.

Limitations of This Study

When working with human samples, several limitations contribute to sources of errors. This experiment's results depended on obtaining samples removed from the operating room and transported back to the Gerstenfeld Laboratory. The length of the surgery and tissue collection depended on which surgeon performed the total arthroplasty, which may have contributed to the variation in results. The time that the reamings were processed directly affects the RIN of each sample. The RNA may have degraded if the sample was left out for too long and not on ice. To fix this, having a larger sample size would eliminate outliers from the results.

Another source of error in this experiment was the cross-contamination of reagents. It is possible that other individuals using reagents led to contamination of RNase, leading to poor RIN values. Along with the reagents, it is possible that some of the tools used in this experiment had traces of RNase on them, leading to degradation. To avoid this, all reagents should be aliquoted separately for each person in the lab. Also, all supplies should be autoclaved the day before surgery to prevent contamination.

The purity of each sample directly affects the qPCR data. As mentioned, the purity of some RNA samples was relatively low based on the 260/280 and 260/230 ratios. The samples with high RINs may have been somewhat contaminated, leading to erroneous measures made during qPCR. To prevent this, allowing the RNA pellet to dry

for longer may be necessary, and resuspending it in water afterward to avoid contamination may be required.

Finally, the sample size of this experiment must be expanded to draw more reliable conclusions. It is possible that several outliers led to skewed data in this experiment. By expanding the sample size, the outliers of the data can be identified and removed from the final results and conclusions. Ultimately this will increase the validity of the results obtained.

Future Experiments

To expand on the findings of this experiment, more patients can be added to the demographics portion of this study to determine comorbidities of osteoporosis and expand the molecular understanding of this disease. In addition to the genes used in this experiment, the following genes may be used to advance this study: Osteocalcin, Runx2, and Osterix.

Finally, to draw more conclusions from the data obtained, Single-cell RNA sequencing can be conducted to understand the individual cells and cellular subpopulations in patients with osteoporosis. This process is highly specific and sensitive to detect the expression of more genes, including those with low expression. Ultimately, the molecular basis of osteoporosis across different populations could be investigated and can lead to the discovery of therapeutic targets for treating and preventing osteoporosis.

BIBLIOGRAPHY

Al-Barghouthi, B. M., & Farber, C. R. (2019). Dissecting the Genetics of Osteoporosis using Systems Approaches. *Trends in genetics : TIG*, *35*(1), 55–67. https://doi.org/10.1016/j.tig.2018.10.004

Ansari, S., Ito, K., & Hofmann, S. (2021). Cell Sources for Human In vitro Bone Models. *Current osteoporosis reports*, *19*(1), 88–100. https://doi.org/10.1007/s11914-020-00648-6

Appelman-Dijkstra, N. M., & Papapoulos, S. E. (2016). Sclerostin Inhibition in the Management of Osteoporosis. *Calcified tissue international*, *98*(4), 370–380. https://doi.org/10.1007/s00223-016-0126-6

Asomaning, K., Bertone-Johnson, E. R., Nasca, P. C., Hooven, F., & Pekow, P. S. (2006). The association between body mass index and osteoporosis in patients referred for a bone mineral density examination. *Journal of women's health (2002)*, *15*(9), 1028–1034. https://doi.org/10.1089/jwh.2006.15.1028

Aspray, T.J., Hill, T.R. (2019). Osteoporosis and the Ageing Skeleton. In: Harris, J., Korolchuk, V. (eds) Biochemistry and Cell Biology of Ageing: Part II Clinical Science. Subcellular Biochemistry, vol 91. Springer, Singapore. https://doi.org/10.1007/978-981-13-3681-2_16

Azzam, E. Z., Ata, M. N., Younan, D. N., Salem, T. M., & Abdul-Aziz, A. A. (2019). DObesity: Relationship between vitamin D deficiency, obesity and sclerostin as a novel biomarker of bone metabolism. *Journal of clinical & translational endocrinology*, *17*, 100197. https://doi.org/10.1016/j.jcte.2019.100197

Barnsley, J., Buckland, G., Chan, P.E. *et al.* Pathophysiology and treatment of osteoporosis: challenges for clinical practice in older people. *Aging Clin Exp Res* **33**, 759–773 (2021). https://doi.org/10.1007/s40520-021-01817-y

Boyle, W. J., Simonet, W. S., & Lacey, D. L. (2003). Osteoclast differentiation and activation. *Nature*, *423*(6937), 337–342. https://doi.org/10.1038/nature01658

Carter, L. E., Kilroy, G., Gimble, J. M., & Floyd, Z. E. (2012). An improved method for isolation of RNA from bone. *BMC biotechnology*, *12*, 5. https://doi.org/10.1186/1472-6750-12-5

Chen, L. R., Ko, N. Y., & Chen, K. H. (2019). Medical Treatment for Osteoporosis:

From Molecular to Clinical Opinions. *International journal of molecular sciences*, *20*(9), 2213. https://doi.org/10.3390/ijms20092213

Demontiero, O., Vidal, C., & Duque, G. (2012). Aging and bone loss: new insights for the clinician. *Therapeutic advances in musculoskeletal disease*, *4*(2), 61–76. https://doi.org/10.1177/1759720X11430858

Feng, J. Q., Ward, L. M., Liu, S., Lu, Y., Xie, Y., Yuan, B., Yu, X., Rauch, F., Davis, S. I., Zhang, S., Rios, H., Drezner, M. K., Quarles, L. D., Bonewald, L. F., & White, K. E. (2006). Loss of DMP1 causes rickets and osteomalacia and identifies a role for osteocytes in mineral metabolism. *Nature genetics*, *38*(11), 1310–1315. https://doi.org/10.1038/ng1905

Ganesan, K., Jandu, J. S., Anastasopoulou, C., Ahsun, S., & Roane, D. (2022). Secondary Osteoporosis. In *StatPearls*. StatPearls Publishing.

Garnero P. (2015). The Role of Collagen Organization on the Properties of Bone. *Calcified tissue international*, *97*(3), 229–240. https://doi.org/10.1007/s00223-015-9996-2

Gkastaris, K., Goulis, D. G., Potoupnis, M., Anastasilakis, A. D., & Kapetanos, G. (2020). Obesity, osteoporosis and bone metabolism. *Journal of musculoskeletal & neuronal interactions*, *20*(3), 372–381.

Gluhak-Heinrich, J., Ye, L., Bonewald, L. F., Feng, J. Q., MacDougall, M., Harris, S. E., & Pavlin, D. (2003). Mechanical loading stimulates dentin matrix protein 1 (DMP1) expression in osteocytes in vivo. *Journal of bone and mineral research : the official journal of the American Society for Bone and Mineral Research*, *18*(5), 807–817. https://doi.org/10.1359/jbmr.2003.18.5.807

Han, Y., You, X., Xing, W., Zhang, Z., & Zou, W. (2018). Paracrine and endocrine actions of bone-the functions of secretory proteins from osteoblasts, osteocytes, and osteoclasts. *Bone research*, *6*, 16. https://doi.org/10.1038/s41413-018-0019-6

Hou, J., He, C., He, W., Yang, M., Luo, X., & Li, C. (2020). Obesity and Bone Health: A Complex Link. *Frontiers in cell and developmental biology*, *8*, 600181. https://doi.org/10.3389/fcell.2020.600181

Huang, W., Yang, S., Shao, J., & Li, Y. P. (2007). Signaling and transcriptional regulation in osteoblast commitment and differentiation. *Frontiers in bioscience : a journal and virtual library*, *12*, 3068–3092. https://doi.org/10.2741/2296

Ji, M. X., & Yu, Q. (2015). Primary osteoporosis in postmenopausal women. *Chronic*

diseases and translational medicine, *1*(1), 9–13. https://doi.org/10.1016/j.cdtm.2015.02.006

Kazley, J., & Bagchi, K. (2022). Femoral Neck Fractures. In *StatPearls*. StatPearls Publishing.

Khosla, S., & Riggs, B. L. (2005). Pathophysiology of age-related bone loss and osteoporosis. *Endocrinology and metabolism clinics of North America*, *34*(4), 1015–xi. https://doi.org/10.1016/j.ecl.2005.07.009

Kim, J. M., Lin, C., Stavre, Z., Greenblatt, M. B., & Shim, J. H. (2020). Osteoblast-Osteoclast Communication and Bone Homeostasis. *Cells*, *9*(9), 2073. https://doi.org/10.3390/cells9092073

Komori T. (2020). What is the function of osteocalcin?. *Journal of oral biosciences*, *62*(3), 223–227. https://doi.org/10.1016/j.job.2020.05.004

Krebs, S., Fischaleck, M., & Blum, H. (2009). A simple and loss-free method to remove TRIzol contaminations from minute RNA samples. *Analytical biochemistry*, *387*(1), 136–138. https://doi.org/10.1016/j.ab.2008.12.020

Li, Y., Xie, B., Jiang, Z., & Yuan, B. (2019). Relationship between osteoporosis and osteoarthritis based on DNA methylation. *International journal of clinical and experimental pathology*, *12*(9), 3399–3407.

Li, X., Ominsky, M. S., Niu, Q. T., Sun, N., Daugherty, B., D'Agostin, D., Kurahara, C., Gao, Y., Cao, J., Gong, J., Asuncion, F., Barrero, M., Warmington, K., Dwyer, D., Stolina, M., Morony, S., Sarosi, I., Kostenuik, P. J., Lacey, D. L., Simonet, W. S., … Paszty, C. (2008). Targeted deletion of the sclerostin gene in mice results in increased bone formation and bone strength. *Journal of bone and mineral research : the official journal of the American Society for Bone and Mineral Research*, *23*(6), 860–869. https://doi.org/10.1359/jbmr.080216

Licini, C., Vitale-Brovarone, C., & Mattioli-Belmonte, M. (2019). Collagen and non-collagenous proteins molecular crosstalk in the pathophysiology of osteoporosis. *Cytokine & growth factor reviews*, *49*, 59–69. https://doi.org/10.1016/j.cytogfr.2019.09.001

Matzkin, E. G., DeMaio, M., Charles, J. F., & Franklin, C. C. (2019). Diagnosis and Treatment of Osteoporosis: What Orthopaedic Surgeons Need to Know. *The Journal of the American Academy of Orthopaedic Surgeons*, *27*(20), e902–e912. https://doi.org/10.5435/JAAOS-D-18-00600

McDonald, M. M., Khoo, W. H., Ng, P. Y., Xiao, Y., Zamerli, J., Thatcher, P., Kyaw, W., Pathmanandavel, K., Grootveld, A. K., Moran, I., Butt, D., Nguyen, A., Corr, A., Warren, S., Biro, M., Butterfield, N. C., Guilfoyle, S. E., Komla-Ebri, D., Dack, M. R. G., Dewhurst, H. F., … Phan, T. G. (2021). Osteoclasts recycle via osteomorphs during RANKL-stimulated bone resorption. *Cell*, *184*(5), 1330–1347.e13. https://doi.org/10.1016/j.cell.2021.02.002

Mirza, F., & Canalis, E. (2015). Management of endocrine disease: Secondary osteoporosis: pathophysiology and management. *European journal of endocrinology*, *173*(3), R131–R151. https://doi.org/10.1530/EJE-15-0118

Porter, J. L., & Varacallo, M. (2022). Osteoporosis. In *StatPearls*. StatPearls Publishing.

Moser, S. C., & van der Eerden, B. C. J. (2019). Osteocalcin-A Versatile Bone-Derived Hormone. *Frontiers in endocrinology*, *9*, 794. https://doi.org/10.3389/fendo.2018.00794

Oliveira, M. C., Vullings, J., & van de Loo, F. A. J. (2020). Osteoporosis and osteoarthritis are two sides of the same coin paid for obesity. *Nutrition (Burbank, Los Angeles County, Calif.)*, *70*, 110486. https://doi.org/10.1016/j.nut.2019.04.001

Pedersen, K. B., Williams, A., Watt, J., & Ronis, M. J. (2019). Improved method for isolating high-quality RNA from mouse bone with RNA*later* at room temperature. *Bone reports*, *11*, 100211. https://doi.org/10.1016/j.bonr.2019.100211

Puchta, M., Boczkowska, M., & Groszyk, J. (2020). Low RIN Value for RNA-Seq Library Construction from Long-Term Stored Seeds: A Case Study of Barley Seeds. *Genes*, *11*(10), 1190. https://doi.org/10.3390/genes11101190

Qiao, D., Li, Y., Liu, X., Zhang, X., Qian, X., Zhang, H., Zhang, G., & Wang, C. (2020). Association of obesity with bone mineral density and osteoporosis in adults: a systematic review and meta-analysis. *Public health*, *180*, 22–28. https://doi.org/10.1016/j.puhe.2019.11.001

Rowe, P., Koller, A., & Sharma, S. (2022). Physiology, Bone Remodeling. In *StatPearls*. StatPearls Publishing.

Salhotra, A., Shah, H. N., Levi, B., & Longaker, M. T. (2020). Mechanisms of bone development and repair. *Nature reviews. Molecular cell biology*, *21*(11), 696–711. https://doi.org/10.1038/s41580-020-00279-w

Sowers, M., Lachance, L., Jamadar, D., Hochberg, M. C., Hollis, B., Crutchfield, M., &

Jannausch, M. L. (1999). The associations of bone mineral density and bone turnover markers with osteoarthritis of the hand and knee in pre- and perimenopausal women. *Arthritis and rheumatism*, *42*(3), 483–489. https://doi.org/10.1002/1529-0131(199904)42:3<483::AID-ANR13>3.0.CO;2-O

Tai, T. W., Li, C. C., Huang, C. F., Chan, W. P., & Wu, C. H. (2022). Treatment of osteoporosis after hip fracture is associated with lower all-cause mortality: A nationwide population study. *Bone*, *154*, 116216. https://doi.org/10.1016/j.bone.2021.116216

Tariq, S., Tariq, S., & Shahzad, M. (2021). Association of serum chemerin with calcium, alkaline phosphatase and bone mineral density in postmenopausal females. *Pakistan journal of medical sciences*, *37*(2), 384–388. https://doi.org/10.12669/pjms.37.2.3907

Tariq, S., Tariq, S., Lone, K. P., & Khaliq, S. (2019). Alkaline phosphatase is a predictor of Bone Mineral Density in postmenopausal females. *Pakistan journal of medical sciences*, *35*(3), 749–753. https://doi.org/10.12669/pjms.35.3.188

Teti A. (2011). Bone development: overview of bone cells and signaling. *Current osteoporosis reports*, *9*(4), 264–273. https://doi.org/10.1007/s11914-011-0078-8

Trajanoska, K., & Rivadeneira, F. (2019). The genetic architecture of osteoporosis and fracture risk. *Bone*, *126*, 2–10. https://doi.org/10.1016/j.bone.2019.04.005

Vimalraj S. (2020). Alkaline phosphatase: Structure, expression and its function in bone mineralization. *Gene*, *754*, 144855. https://doi.org/10.1016/j.gene.2020.144855

Vasiliadis, E. S., Evangelopoulos, D. S., Kaspiris, A., Benetos, I. S., Vlachos, C., & Pneumaticos, S. G. (2022). The Role of Sclerostin in Bone Diseases. *Journal of clinical medicine*, *11*(3), 806. https://doi.org/10.3390/jcm11030806

Wang, J. S., Mazur, C. M., & Wein, M. N. (2021). Sclerostin and Osteocalcin: Candidate Bone-Produced Hormones. *Frontiers in endocrinology*, *12*, 584147. https://doi.org/10.3389/fendo.2021.584147

Watts, N. B., & Diab, D. L. (2010). Long-term use of bisphosphonates in osteoporosis. *The Journal of clinical endocrinology and metabolism*, *95*(4), 1555–1565. https://doi.org/10.1210/jc.2009-1947

Wu, H., Teng, P. N., Jayaraman, T., Onishi, S., Li, J., Bannon, L., Huang, H., Close, J., & Sfeir, C. (2011). Dentin matrix protein 1 (DMP1) signals via cell surface integrin. *The Journal of biological chemistry*, *286*(34), 29462–29469.

https://doi.org/10.1074/jbc.M110.194746

Xing, R. L., Zhao, L. R., & Wang, P. M. (2016). Bisphosphonates therapy for osteoarthritis: a meta-analysis of randomized controlled trials. *SpringerPlus*, *5*(1), 1704. https://doi.org/10.1186/s40064-016-3359-y

Yang, TL., Shen, H., Liu, A. *et al.* A road map for understanding molecular and genetic determinants of osteoporosis. *Nat Rev Endocrinol* **16**, 91–103 (2020). https://doi.org/10.1038/s41574-019-0282-7

Zhang, Y. B., Zhong, Z. M., Hou, G., Jiang, H., & Chen, J. T. (2011). Involvement of oxidative stress in age-related bone loss. *The Journal of surgical research*, *169*(1), e37–e42. https://doi.org/10.1016/j.jss.2011.02.033

Zhou, S., Huang, G., & Chen, G. (2020). Synthesis and biological activities of drugs for the treatment of osteoporosis. *European journal of medicinal chemistry*, *197*, 112313. https://doi.org/10.1016/j.ejmech.2020.112313

CURRICULUM VITAE